Karson, J.A., Cannat, M., Miller, D.J., and Elthon, D. (Eds.), 1997
Proceedings of the Ocean Drilling Program, Scientific Results, Vol. 153

5. LOCALIZATION OF DUCTILE STRAIN AND THE MAGMATIC EVOLUTION OF GABBROIC ROCKS DRILLED AT THE MID-ATLANTIC RIDGE (23°N)[1]

Mathilde Cannat,[2] Georges Ceuleneer,[3] and John Fletcher[4]

ABSTRACT

Ductile deformation of gabbroic rocks drilled on the west wall of the Mid-Atlantic Ridge south of the Kane Fracture Zone (Sites 921–923) localizes preferentially in gabbronoritic intervals. The least evolved gabbroic lithologies (troctolites) are rarely deformed, and the most evolved ones (leucocratic segregations) are not deformed. A close look at ductile shear zones and at their mineral chemistry suggests that, in many cases, they developed in gabbronoritic dikelets intruded into less evolved lithologies. Recrystallized phase assemblages are similar to igneous ones in most deformed samples. This indicates that ductile deformation occurred in high-temperature nearly anhydrous conditions similar to magmatic conditions. Compositional variations in igneous and recrystallized minerals in many shear zones also suggest that ductile deformation took place with some residual melt present. The presence of interstitial melt in shear zones during deformation would produce a strong rheological contrast between material in the shear zone and the surrounding rocks. The range of gabbroic lithologies drilled at Sites 921–923, their relative proportions in the core, the composition of igneous minerals, the preferred localization of ductile deformation in gabbronoritic lithologies, and the probable role of trapped fractionated melts in favoring this strain localization recall observations made in gabbroic rocks from Site 735 in the Southwest Indian Ocean.

INTRODUCTION

Gabbroic rocks exposed along the median valley walls of mid-ocean ridges represent magmas that pooled and crystallized at some depth below the axial seafloor and were subsequently exhumed and emplaced into the upper crust. These rocks give us an opportunity to study processes active in the deep axial magma plumbing system, a system that is commonly out of the reach of sampling techniques and can only be approached through geophysical experiments.

The emplacement of gabbroic rocks to the seafloor is restricted to portions of the world ridge system that have a deep and wide axial valley and that commonly are near axial, transform or "non-transform" discontinuities. This is the case for the gabbroic exposures of the Mid-Atlantic Ridge near the Kane Fracture Zone (MARK area; Fig.1). Submersible studies in this region (Dick et al., 1981; Karson et al., 1987; Mével et al., 1991; Auzende et al., 1993) have shown that the gabbroic rocks are exposed along low-dipping normal fault planes. These fault surfaces were drilled through during Leg 153 and extensively cataclased fault rocks were recovered in the core (Cannat, Karson, Miller, et al., 1995). The existence of such faults and the accentuated relief of the axial valley are both consistent with the hypothesis that plate divergence in this region, and more generally in regions where rocks that formed deep below the seafloor (serpentinized peridotites or gabbroic rocks) are exposed in the seafloor, involves a large component of tectonic extension (Dick et al., 1981; Karson et al., 1987; Karson, 1990; Cannat, 1993). If this is indeed the case, there must be evidence for tectonic extension not only in the uppermost, brittle part of the axial lithosphere, but also in its deeper and hotter parts. Rocks that have been exhumed from these deeper lithospheric levels should therefore be affected by high-temperature, brittle-ductile, and ductile extensional deformation.

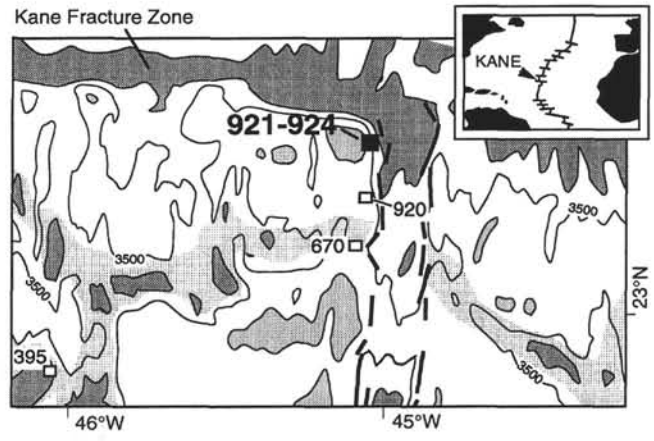

Figure 1. Simplified bathymetric map of the MARK area (after Gente et al., 1995) showing the location of Sites 395 (Deep Sea Drilling Project Leg 45; serpentinized peridotites and gabbro), 670 (ODP Leg 109; serpentinized peridotites), 920 (Leg 153; serpentinized peridotites and gabbro), and 921–924 (this study). Bathymetric contours: 4000 m (domains deeper than 4000 m in dark gray), 3500 m, and 2500 m (domains shallower than 2500 m in lighter gray). Heavy lines show the median valley main scarps. Alignments of basins, interpreted as marking the off-axis trace of axial discontinuities, are outlined in an intermediate shade of gray.

Drilling at Site 735 during Ocean Drilling Program (ODP) Leg 118 provided ample evidence for such high-temperature extensional deformation in exhumed gabbroic rocks from the Southwest Indian Ridge (Cannat et al., 1991; Dick et al., 1991). A large proportion of the gabbroic rocks that have been sampled during submersible, dredging, or during other drilling legs in various parts of the world's slow-spreading ridge system are similarly deformed (Helmstaedt and Allen, 1977; Ito and Anderson, 1983; Mével and Cannat, 1991; Cannat and Casey, 1995).

[1]Karson, J.A., Cannat, M., Miller, D.J., and Elthon, D. (Eds.), 1997. *Proc. ODP, Sci. Results,* 153: College Station, TX (Ocean Drilling Program).

[2]Laboratoire de Pétrologie-URA CNRS 736, Université Pierre et Marie Curie, 4 place Jussieu, 75252 Paris cedex 05, France. mac@ccr.jussieu.fr

[3]Observatoire Midi-Pyrénées, CNRS-UPR 234, 14 av. E. Belin, 31400 Toulouse, France.

[4]Departamento de Geologia, CICESE P.O. Box 434843, San Diego, CA 92143-4843, U.S.A.

Gabbroic core totaling 78.5 m was recovered during Leg 153 on the west wall of the Mid-Atlantic Ridge axial valley, a few kilometers to the south of the Kane Fracture Zone (Fig. 1). These gabbroic rocks show striking similarities to the Site 735 rocks, both in terms of mineralogy and magmatic evolution (Ross and Elthon, this volume; Casey, this volume; this study) and of deformational microstructures (Fletcher, Ceuleneer, et al., this volume). The core from the MARK area sites is, however, not nearly as extensively sheared as the core from Site 735. Meter- to decameter-thick intervals of gabbroic ductile mylonites were recovered at Site 735. Mylonitic gabbros drilled at the MARK sites form decimeter-thick intervals at most (Fig. 2). Although not as spectacular in terms of displacement as the mylonites recovered from Site 735, these thin shear zones give us the opportunity to study the initial stages of ductile strain localization in the gabbros and their relationships with fine-scale magmatic features in the core.

Many mylonitic shear zones in the gabbroic rocks drilled at Site 735 in the southwest Indian Ocean occur in evolved oxide-bearing gabbros, suggesting an interplay between the localization of ductile deformation and the distribution of fractionated melts in the solidifying gabbro pile (Bloomer et al., 1991; Dick et al., 1991). Our aim in this paper is to check whether a comparable interplay existed in the MARK area gabbroic rocks. We have examined the mineralogy of ductile shear zones cored at Sites 921–923, and conducted detailed microprobe analyses of igneous and dynamically recrystallized minerals in a set of samples selected after a macroscopic survey of the core and after viewing about 300 thin sections (the shipboard thin sections listed in Cannat, Karson, Miller, et al., 1995, and the set of thin sections studied by Fletcher, Ceuleneer, et al., this volume). We believe that these selected samples are representative of the mineralogical variety in ductile shear zones that have been recovered at Sites 921–923. Over 70% of the material drilled in the eight shallow holes at these sites has, however, not been recovered (Table 1; Cannat, Karson, Miller, et al., 1995). This lost material presumably also included ductile shear zones, some of which may have been different from those that have been recovered. The results presented in this paper will be discussed with this limitation in mind.

DUCTILE SHEAR ZONES: IGNEOUS AND RECRYSTALLIZED MINERALOGY

The gabbroic rocks cored at the MARK area sites are troctolites, olivine gabbros (volumetrically the predominant rock type), gabbros, gabbronorites, oxide gabbronorites, olivine gabbronorites, and norites, as well as small volumes of leucocratic, commonly quartz-bearing, segregates (Cannat, Karson, Miller, et al., 1995). This range of mineralogy, similar to that sampled at Site 735 in the Southwest Indian Ocean (Shipboard Scientific Party, 1989), corresponds to a wide range of mineral compositions and to large differences in the degree of magmatic fractionation. Again, similar to what was observed at Site 735, these various rock types are interspersed over short lengths of core (at scales of a few centimeters to a few meters) in no stratigraphic order.

Igneous Mineralogy and the Distribution of Ductile Strain

The downhole distribution and the fabrics of deformed intervals at Sites 921, 922, and 923 are described by Fletcher, Ceuleneer, et al. (this volume). Here, we use a simplified version of the textural systematics described in their paper, based on the proportion of plagioclase grains that we infer to be dynamically recrystallized: 0% recrystallized plagioclase corresponds to textural type 1; <30%, 30%–70%, 70%–90%, and >90% recrystallized plagioclase correspond to textural types 1, 2, 3, and 4, respectively.

We use this proportion of recrystallized over igneous plagioclase as a qualitative indicator of the intensity of ductile deformation in our samples. Plagioclase grains that we interpret as dynamically recrystallized are smaller than the surrounding igneous plagioclase, and are equant as well as commonly polygonal in shape. Their size is variable, possibly reflecting variations of the physical conditions during ductile deformation (Cannat, Karson, Miller, et al., 1995; Fletcher, Ceuleneer, et al., this volume). In samples that contain more than 30% recrystallized plagioclase, igneous grains of olivine and pyroxene are commonly surrounded by smaller equant and polygonal grains of the same minerals also inferred to be dynamically recrystallized. The reader is referred to Fletcher, Ceuleneer, et al. (this volume) for microstructural details and for a discussion of deformation mechanisms. The textural systematics we use here are based on plagioclase because it is present in large amounts in all gabbroic lithologies, and because it appears to be dynamically recrystallized in all deformed samples (Cannat, Karson, Miller, et al., 1995; Fletcher, Ceuleneer, et al., this volume).

Table 2 and Figure 3 show that there is a definite correlation, in gabbroic rocks from Sites 921 to 923, between igneous mineralogy and the degree of plagioclase recrystallization (inferred to give an indication on the amount of ductile strain). Troctolites represent 18.4% of the 315 gabbroic samples we have examined in thin sections. 43.1% of these troctolitic samples do not contain recrystallized plagioclase, and plagioclase in 87.9% of these samples is less than 30% recrystallized (Fig. 3). By contrast, the proportion of recrystallized plagioclase is more than 70% in 68.6% of gabbronoritic samples (gabbronorites, oxide gabbronorites, olivine gabbronorites, and norites), and only 3.9% of these gabbronoritic samples do not contain recrystallized plagioclase. Ductile deformation, therefore, appears to have localized preferentially in gabbronoritic intervals, most of the less-evolved troctolites and olivine gabbros being weakly deformed or undeformed. Leucocratic segregations are systematically undeformed.

The distribution of igneous lithologies and of textural types listed for the 315 gabbroic samples considered in Table 2 is not representative of the gabbroic section recovered at Sites 921–923. It is biased toward the more deformed samples, and, therefore, it also overestimates the proportion of gabbronoritic intervals. The relative proportions of igneous lithologies, and of textural types in a subset of these 315 samples that corresponds to the thin sections made on board the *JOIDES Resolution* during Leg 153 (Cannat, Karson, Miller, et al., 1995), are probably closer to actual proportions in the recovered gabbroic section. In this subset of samples (132 samples; Table 2), gabbroic rocks with no recrystallized plagioclase represent 44.7%, whereas sheared intervals with more than 70% recrystallized plagioclase represent only 8.4%.

Ductile Shear Zones: Macroscopic Description and Mineral Assemblages

Intervals of pronounced ductile deformation (textural types 3 and 4) have a well-defined foliation (Fig. 2). They are commonly only a few millimeters to a few centimeters thick (Fig. 2A). The decimeter-thick shear zones shown in Figures 2B and 2C are uncommon features in the core. There are, however, moderately deformed (textural type 2), weakly foliated intervals of gabbro and olivine gabbro that extend over a few meters of core (Cannat, Karson, Miller, et al., 1995).

Some shear zones develop in oxide-bearing intervals (Fig. 2A), others develop in oxide-free lithologies. There are also centimeter-thick intervals of oxide-bearing gabbro that form dikelets and seams in the surrounding rocks and are undeformed, or are weakly foliated (Fig. 4), with moderately recrystallized plagioclase (textural type 2). The mineralogical characteristic shared by most deformed intervals

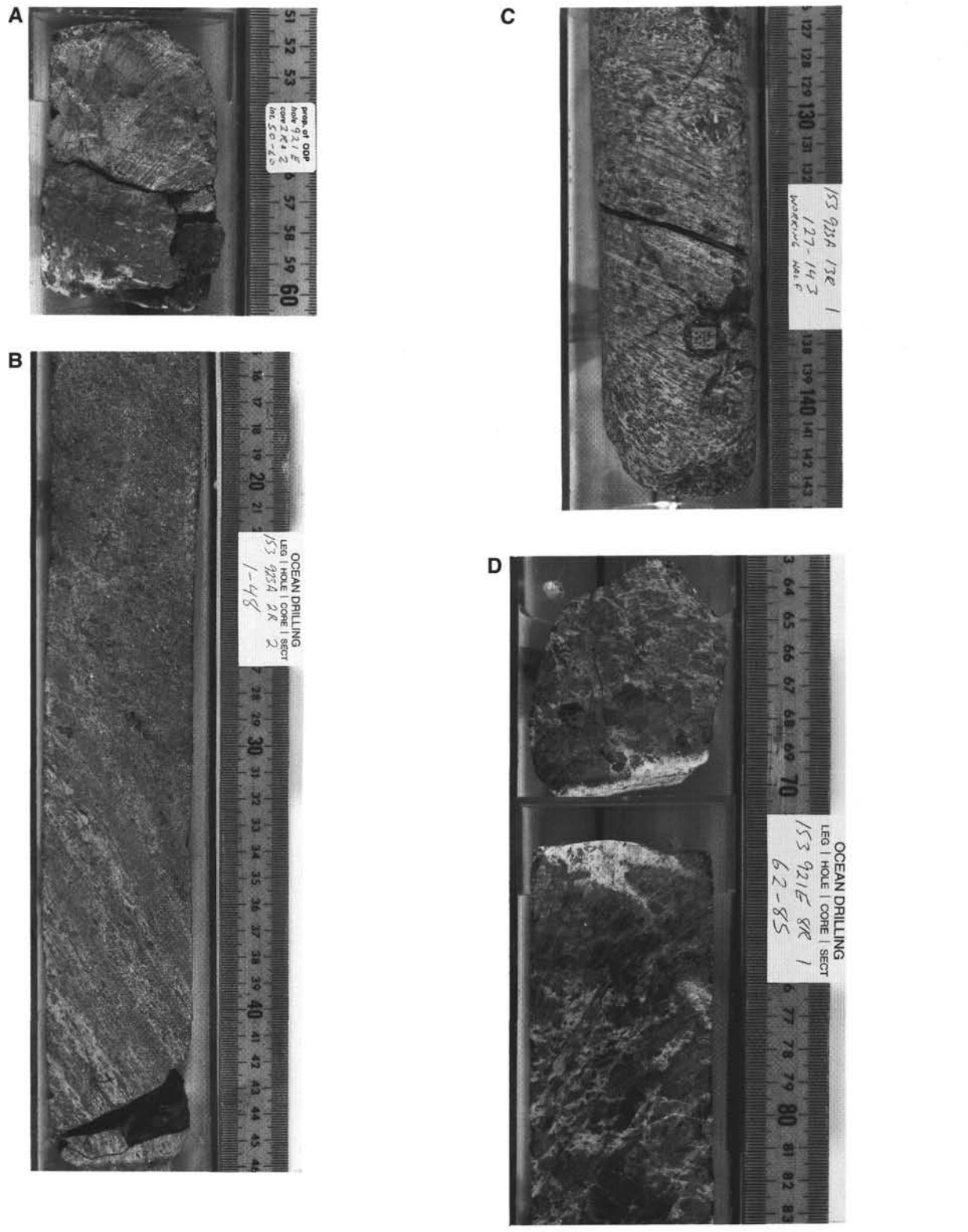

Figure 2. Core photographs. **A.** Sample 153-921E-2R-2, 51–60 cm. Mylonitic interval of oxide gabbronorite (57–60 cm) in weakly deformed coarse-grained olivine gabbro (51–57 cm). **B.** Sample 153-923A-2R-2, 22–45 cm. Shear zone with steep foliation cutting through undeformed olivine gabbro (22–37 cm on right side of photograph). The shear zone contains bands of finely recrystallized olivine-bearing microgabbronorite and coarser grained bands (lighter in photograph) of foliated gabbronorite. **C.** Sample 153-923A-13R-1, 126–142 cm. Shear zone with low-dipping foliation developed in medium-grained olivine gabbro (less deformed intervals), and finer grained gabbronorite (photomicrographs in Figs. 5D, 5F). **D.** Interval 153-921E-8R-1, 64–83 cm. Moderately deformed, coarse-grained olivine-bearing gabbro with white seams that outline an irregular foliation and that are produced by recrystallized plagioclase and by undeformed, fine-grained leucocratic segregations, along grain boundaries, and in fractures (similar to photomicrograph in Fig. 5C). Coarser grained, undeformed leucocratic segregations form a vein at 69–73 cm.

Table 1. Location and drilling record from Sites 921 to 923 (Cannat, Karson, Miller, et al., 1995).

Hole	Latitude (N)	Longitude (W)	Cored (mbsf)	Recovered (m)
921A	23°32.46′	45°01.86′	17.1	3.1
921B	23°32.48′	45°01.84′	44.1	10.2
921C	23°32.47′	45°01.83′	53.4	6.1
921D	23°32.44′	45°01.83′	48.6	6.16
921E	23°32.33′	45°01.88′	82.6	17.65
922A	23°31.37′	45°01.92′	14.6	9.23
922B	23°31.37′	45°01.92′	37.4	11.9
923A	23°32.55′	45°01.89′	70.0	40.7

Note: mbsf = meters below seafloor.

with type 3 or 4 textures is that they contain orthopyroxene, as igneous porphyroclasts, recrystallized grains, or both (Table 3).

Ductile shear zones at Sites 921–923 also typically have sharp contacts with the surrounding, less deformed to undeformed, gabbroic rocks (Figs. 2A, 5A, 5D), and these contacts commonly coincide with lithological contacts. Samples selected for microprobe analyses in this paper commonly include such deformational and lithological contacts (Table 3). Consistent with the data shown in Table 2, many of these contacts involve troctolites or olivine gabbro on the undeformed to weakly deformed side, and gabbronoritic lithologies on the strongly deformed side (Figs. 2A, 5A, 5D; Table 3). In many samples, there also is a marked change in the size of igneous minerals across these deformational and lithological contacts, the most deformed material containing smaller igneous minerals. Smaller igneous grain sizes in the most deformed intervals could result from recrystallization. It is, however, common to observe in the recrystallized matrix small pyroxene grains that have retained euhedral igneous shapes (Figs. 5D, 5E) and may therefore be representative of original igneous grain sizes. There are occasional dikelets of fine-grained gabbronorite in the core (e.g., Sample 153-12R-2, 26–31 cm) that may represent the protolith for such fine-grained sheared intervals.

Deformed gabbroic rocks with type 3 and 4 textures commonly contain microscopic patches of fine-grained undeformed leucocratic material, with rectangular-shaped plagioclase, interstitial brown to green amphibole, occasional quartz, zircon, and apatite (Fig. 5B). These leucocratic segregations are similar to lithologies sampled at Site 735 (Dick et al., 1991) and interpreted there as the product of crystallization of trapped residual melt. Most leucocratic segregations do not contain clinopyroxene, either because it was never present, or because it has been replaced by brown to greenish brown amphibole. The origin, late magmatic or hydrothermal, of this amphibole is not clear. Sample 153-923A-2R-2, 30–33 cm, contains a few flakes of biotite that are bent but not recrystallized and line the contact between undeformed gabbro and extensively recrystallized gabbronorite (Table 3). The origin of this biotite is also unclear. Undeformed leucocratic segregations also fill intergranular interstices and fractures in some moderately deformed gabbroic rocks (Fig. 5C), producing a characteristic pattern of white seams in the rock (Fig. 2D). Coarser grained leucocratic segregations form centimeter-thick veins in deformed (Fig. 2D) and undeformed gabbros (e.g., Sample 153-921E-7R-2, 94–100 cm; Table 3).

The dynamically recrystallized assemblage in deformed gabbroic rocks with type 3 and 4 textures includes plagioclase, pyroxene, and olivine, as well as small amounts of brown amphibole (commonly <1%), titanium oxide and apatite. The brown amphibole, interpreted here as magmatic, is the only recrystallized hydrous phase in most samples. It occurs as polygonal or interstitial grains in the recrystallized aggregates (Figs. 5D, 5F). Brownish green to green amphiboles that fill microfractures or develop as hydrothermal alteration products of igneous and recrystallized minerals are most commonly undeformed. One exception is a 1-cm-thick zircon-bearing shear zone in Sample 153-922B-4R-1, 67–74 cm (Table 3), that contains recrystallized green amphibole. Recrystallized clinopyroxene is present in all shear zones, except in noritic samples (Table 3). Recrystallized orthopyroxene is also common (Table 3). Olivine occurs as porphyroclasts and neoblasts rimmed with small polygonal orthopyroxene grains (Fig. 5F). Rims of undeformed orthopyroxene around olivine grains occur as an igneous texture in the MARK area gabbroic core, possibly reflecting late magmatic interactions between the olivine gabbro and a residual melt comparatively enriched in silica and/or water. Less commonly, olivine is rimmed by complex intergrowths of iron oxide and orthopyroxene. This last texture is clearly reactional and occurs in olivine-bearing gabbros that have been injected by late magmatic leucocratic segregates (e.g., Sample 153-921E-3R-1, 25–30 cm). Polygonal orthopyroxene grains that surround olivine in sheared olivine gabbros (Fig. 5F) could be produced by the recrystallization of rims of late magmatic orthopyroxene, or by synkinematic reaction between the deforming olivine-bearing gabbro and a silica- and/or water-rich fluid.

DUCTILE SHEAR ZONES: COMPOSITION OF IGNEOUS AND RECRYSTALLIZED MINERALS

Microprobe analyses were performed using the CAMEBAX "Camparis" probe (Université de Paris VI), with a beam current of 40 nA, a voltage of 15 V, counting times of 10 to 20 s, and a defocused beam for plagioclase analyses. Selected analyses are presented in Tables 4 through 6.

Compositional Trends in Igneous Clinopyroxene and Plagioclase

Undeformed and weakly deformed (textural types 0 and 1) gabbroic rocks cored at Sites 921–923 show a wide range of igneous mineral compositions, comparable to the range measured in gabbroic rocks from the Southwest Indian Ocean (Fig. 6). This wide range of mineral compositions is consistent with the wide range of recovered gabbroic lithologies, and suggests extensive differentiation along a tholeiitic trend. Troctolites contain the most magnesium-rich clinopyroxenes and the most An-rich plagioclase and would be the first crystallization products along this trend. Leucocratic segregations plot at the other end of the compositional spectrum, with low plagioclase An contents, and clinopyroxene that, when present, has Mg# values ($Mg/[Mg + Fe_{tot}]$) as low as 0.64 (Fig. 6).

Most deformed (textural types 2, 3, and 4) gabbroic rocks cored at Sites 921–923 also plot on the clinopyroxene Mg# vs. An% plagioclase tholeiitic differentiation trend (Fig. 6). They have a more restricted range of compositions than undeformed or weakly deformed samples because the most-evolved igneous assemblages (leucocratic segregations) are never deformed and the least-evolved igneous assemblages (troctolites) are rarely deformed (Table 2). The deformed troctolites selected for this study (Samples 153-922A-2R-2, 106–111 cm, and 153-922B-1W-1, 109–115 cm; Table 3) do not contain clinopyroxene, but they contain plagioclase with An contents up to 80%.

Compositional trends in igneous clinopyroxene and plagioclase from samples listed in Table 3 are shown in Figures 7 and 8. These compositional trends are consistent with trends of increasing magmatic differentiation and very similar to trends measured in gabbroic core from Site 735 in the Southwest Indian Ridge (Bloomer et al., 1991; Ozawa et al., 1991).

Clinopyroxene in the least-evolved, undeformed to weakly deformed troctolites and olivine gabbros has variable titanium (up to 1.6%) and aluminum contents (Fig. 7). The igneous clinopyroxene analyzed in the extensively recrystallized (textural type 4) gab-

Table 2. Igneous lithology and textural type in gabbroic rocks from Sites 921 to 923.

	0		1		2		3		4		Total		Subset	
Textural type:	A	B (%)	A	B (%)	A	B (%)	A	B (%)	A	B (%)	A	C (%)	A	C (%)
Troctolite	25	43.1	26	44.8	3	5.2	3	5.2	1	1.7	58	18.4	30	22.7
Ol gabbro	36	28.1	30	23.4	39	30.4	18	14.1	5	3.9	128	40.6	55	41.7
Gabbro	15	23.8	15	23.8	21	33.3	7	11.1	5	7.9	63	20.0	28	21.2
Gabbronorite	2	3.9	9	17.6	5	9.8	17	33.3	18	35.3	51	16.2	14	10.6
Leuc. segreg.	15	100	0	0	0	0	0	0	0	0	15	4.7	5	3.8
Total	93	29.5	80	25.4	68	21.6	45	14.3	29	9.2	315			
Subset	59	44.7	33	25.0	29	21.9	10	7.6	1	0.7			132	

Notes: Textural type corresponds to degree of recrystallization of plagioclase (see text). Data are from 315 gabbroic samples from Sites 921 to 923, and a subset of 132 samples used for shipboard thin sections (Cannat, Karson, Miller, et al., 1995). Column A lists the number of samples in each textural type; column B lists the percentage of samples in each textual type; column C lists the percentage of samples of each lithology in the set of samples analyzed. Gabbronorite is used as a general term that includes gabbronorites, oxide gabbronorite, olivine gabbronorites, and norites. Ol = olivine, Leuc. segreg. = leucocratic segregation.

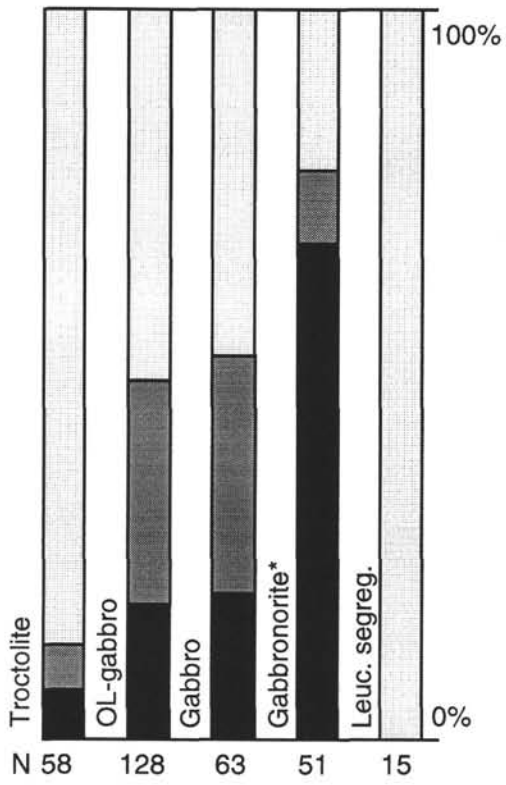

Figure 3. Histogram showing the proportion of recrystallized plagioclase in the different gabbroic lithologies sampled at Sites 921–923. Gabbronorites* = gabbronorites, oxide gabbronorites, olivine gabbronorites, and norites. N = numbers of samples of each lithology (see Table 2). Leuc. segreg. = leucocratic segregation. Light gray: less than 30% of plagioclase is recrystallized (textural types 0 and 1); dark gray: 30%–70% (textural type 2); black: >70% (textural types 3 and 4).

bronoritic interval in Sample 153-922A-2R-2, 56–62 cm (Table 3), has less titanium (about 0.4%), sodium, and chromium for a similarly high Mg# (Table 4). This gabbronoritic interval also contains igneous plagioclase with relatively low An contents and therefore plots well above the tholeiitic differentiation trend in Figure 6. In clinopyroxenes with Mg# lower than about 0.82, titanium content first increases with decreasing Mg#, up to 1% for Mg# values of about 0.74 (Fig. 7), then decreases markedly, reaching values of less than 0.5% in some gabbronoritic samples and in the leucocratic segregation of Sample 153-923A-2R-6, 18–25 cm, and of less than 0.25% in leucocratic segregations of Samples 153-921E-7R1, 25–29 cm, and 153-923A-16R-4, 85–89 cm (Table 3). These titanium-poor clinopyroxenes also have low aluminum contents (Fig. 7). In some gabbronoritic samples, they coexist with clinopyroxenes that have similar Mg#, but higher titanium and aluminum contents (e.g., Samples 153-921E-3R-1, 3–9 cm, and 153-921B-3R-1, 134–137 cm).

Potassium content in plagioclase (Fig. 8) increases slowly with decreasing anorthite contents, reaching values of about 0.3% K_2O in most plagioclase from leucocratic segregations. Quartz-bearing segregations also contain small amounts of sodium-rich plagioclase with up to 0.82% K_2O. Igneous plagioclase in the strongly deformed, orthopyroxene-bearing intervals of Samples 153-922A-3R-1, 63–66 cm, and 153-922B-1W-1, 109–115 cm, have high An contents (up to 80%; Table 3). The strongly deformed interval in Sample 153-922B-1W-1, 109–115 cm, is troctolitic and contains no relics of igneous clinopyroxene. The deformed gabbronorite in Sample 153-922A-3R-1, 63–66 cm, contains clinopyroxene with low Mg#, and therefore plots well below the tholeiitic differentiation trend in Figure 6.

Composition of Recrystallized Minerals

Igneous and recrystallized plagioclase have similar average An contents in most samples (Table 5; Fig. 9A). The four samples (Samples 153-921E-3R-1, 3–9 cm, 153-921E-7R-2, 70–75 cm, 153-922A-2R-6, 18–25 cm, and 153-922A-3R-1, 63–66 cm) that contain recrystallized plagioclase that is, on average, enriched in sodium compared with igneous grains also plot off the tholeiitic differentiation trend, toward higher An contents, or lower Mg#, in Figure 6, a diagram of igneous clinopyroxene Mg# vs. igneous plagioclase An content. In these four samples, the range of An contents in recrystallized plagioclase is large (Table 3; Fig. 9A).

Igneous and recrystallized clinopyroxene (Table 4; Fig. 9B) and olivine (Table 6) are compositionally similar in all samples. Values of Mg# in igneous orthopyroxene from some deformed gabbronoritic samples vary over a wide range (Table 3). The range of Mg# values is similar or smaller in recrystallized orthopyroxenes. These samples plot off the 1:1 trend in Figure 9C: average values of Mg# in orthopyroxene neoblasts are either higher (Samples 153-921E-2R-2, 54–60 cm, 153-922A-3R-1, 3–9 cm, and 153-922B-1W-1, 109–115 cm), or lower (Sample 153-921E-7R-2, 70–75 cm), than in igneous orthopyroxene. Two of these samples (Samples 153-921E-7R-2, 70–75 cm, and 153-922A-3R-1, 3–9 cm) also plot off the tholeiitic differentiation trend in Figure 6. In other deformed samples, igneous and recrystallized orthopyroxenes are compositionally similar (Table 6; Fig. 9C).

Brown amphiboles that form interstitial grains and polygonal neoblasts in dynamically recrystallized samples (Figs. 5D, 5F) are titanium-rich hornblendes and less common pargasitic hornblendes (Fig. 10). They are compositionally similar to brown amphiboles that we interpret as magmatic, and that form small inclusions in igneous clinopyroxene, or rims around olivine and pyroxene crystals in undeformed gabbros. Variations in magnesium, chromium, and titanium contents in these brown amphiboles (Fig. 10) reflect the composition of igneous clinopyroxenes in each studied sample (Fig. 7). Pale

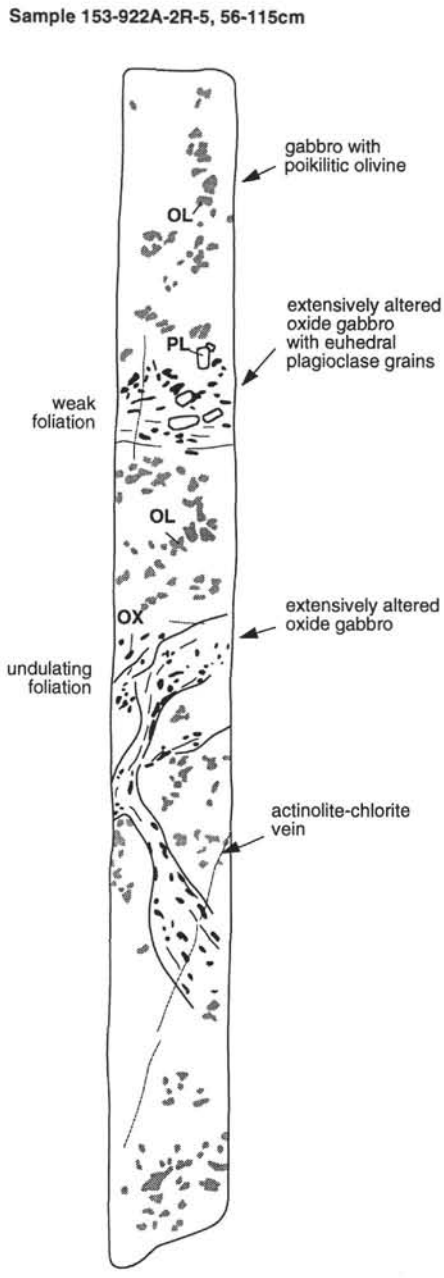

Figure 4. Sketch of the relationships between undeformed olivine gabbro and poikilitic olivine, and foliated to undeformed seams of oxide gabbronorite and norite in Sample 153-922A-2R–5, 56–115 cm. The orientation of the foliation in oxide-bearing intervals is controlled by the geometry of their contacts with the undeformed olivine gabbro. Core is 5.5 cm in diameter. OL = olivine, PL = plagioclase, OX = Fe-Ti oxide.

brown to green actinolite and actinolitic hornblende (Fig. 10) crystallized as interstitial crystals in undeformed leucocratic segregations and as dynamically recrystallized grains in the zircon-bearing, 1-cm-thick shear zone of Sample 153-922B-4R-1, 67–74 cm (textural type 4; Table 3). Undeformed actinolitic amphiboles that occur in microfractures or as replacement for igneous minerals are not considered in this study because their crystallization postdated ductile deformation (with the exception of Sample 153-922B-4R-1, 67–74 cm). Selected microprobe analyses for these amphiboles are, however, listed in Table 6.

A DISCUSSION OF MELT-ROCK CHEMICAL INTERACTIONS IN AND NEAR SHEAR ZONES

Ductile shear zones at Sites 921–923 commonly developed in thin (millimeter- to decimeter-thick) gabbronoritic intervals, and have sharp contacts with less deformed to undeformed troctolites, olivine gabbros, or gabbros. Many of our sheared samples include one such contact (Table 3). Igneous minerals in deformed and less deformed lithologies near these contacts commonly have a wide range of compositions (e.g., Table 3). Average clinopyroxene and plagioclase compositions in some deformed samples plot off the tholeiitic differentiation trend, either toward higher plagioclase An contents or, in one case, toward higher clinopyroxene Mg# values (Figs. 6, 11A). Average Mg# values for igneous olivine do plot near the olivine/plagioclase differentiation trend (Fig. 11B), but the range of olivine Mg# in deformed and less deformed lithologies is large (Table 3). Igneous orthopyroxene in deformed samples commonly plots off the orthopyroxene/plagioclase differentiation trend (Fig. 11C): igneous orthopyroxene Mg# values are too low at a given plagioclase An content. In two of the four samples that contain a contact between two igneous orthopyroxene-bearing lithologies, we observe, however, that igneous orthopyroxene in the most deformed part of the sample has Mg# values that are too high at a given plagioclase An content.

We interpret these chemical complexities as caused by melt-rock chemical interactions in and near the shear zones. In the following paragraphs, we use Samples 153-922A-2R-2, 56–62 cm, and 153-921E-7R-2, 70–75 cm, to discuss these chemical interactions.

The shear zone in Sample 153-922A-2R-2, 56–62 cm, contains sodium-rich plagioclase and occasional relics of fine-grained igneous clinopyroxene and orthopyroxene (Figs. 6, 11A, 11B) and is a 5-mm-thick interval of mylonitic gabbronorite. The texture of this thin shear zone is similar to that shown in Figure 5D. This gabbronorite appears to have originally been a dikelet, cutting through an undeformed olivine gabbro (Table 3). The olivine gabbro contains high-magnesium olivine (Fig. 11B) and minor orthopyroxene that rims the olivine (Fig. 11C). Pyroxenes in the deformed gabbronorite also have high Mg# values, but clinopyroxene chromium, aluminum, and titanium contents are much lower than in the olivine gabbro (Table 4). We propose that, in this sample, the Mg# of the melt that crystallized the gabbronorite had been buffered by the magnesium-rich host gabbro.

In contrast, the shear zone in Sample 153-921E-7R-2, 70–75 cm (Fig. 5A), contains sodium-poor plagioclase porphyroclasts and iron-rich igneous clinopyroxene (Figs. 6, 11A). It is a 3-cm-thick interval of mylonitic gabbronorite with angular to rounded xenocrysts of clinopyroxene, plagioclase, and olivine from the surrounding undeformed olivine gabbro (Fig. 5A). Igneous pyroxenes in the gabbronorite are fine-grained and commonly euhedral (Fig. 5E). Recrystallized plagioclase forms small polygonal to anhedral grains that surround ribbon-shaped debris of igneous porphyroclasts (Fig. 5E). There are also small tablet-shaped plagioclase grains (similar to those shown in Fig. 5C) that are associated with interstitial amphibole and zircon in thin leucocratic segregations.

In Figure 6, we have plotted the average An content (64.1%) measured in ribbon-shaped plagioclase porphyroclasts in Sample 153-921E-7R-2, 70–75 cm. An contents are much smaller in tablet-shaped plagioclase from the leucocratic segregations (24.6% on average; Table 3) and intermediate, with a large range of variation (25.2%–53.2%) in recrystallized plagioclase (Fig. 9A). An contents in plagioclase cores from the undeformed olivine gabbro near the shear zone are also variable (68.2%–76.1%; Table 3), with a 69.1% average value. We propose that the ribbon-shaped plagioclase porphyroclasts in Sample 153-921E-7R-2, 70–75 cm, and, more generally, in shear zones that plot below the plagioclase/clinopyroxene differentiation trend in Figure 6 are in fact highly deformed plagioclase xenocrysts from the less-evolved surrounding gabbro. Plagioclase

Table 3. Gabbroic samples microprobed for this study, with a summary of their mineral composition.

Core, section, interval (cm)	Mineralogy	Text. type	Average mineral composition						
			Pl	Cpx	Opx	Ol	Pl (R)	Cpx (R)	Opx (R)
			An%	Mg#	Mg#	Mg#	An%	Mg#	Mg#
921B-3R-1, 33–36	Gabbronorite, ox, am	3	46.46	66.72	62.04		45.41		
921B-3R-1, 71–79	Ol gabbro, am, opx	3	57.31	77.35	71.29	68.68	50.01	74.59	
	Gabbronorite, ox, am, ap	3	45.74	67.51	59.16		49.75	66.35	60.52
921B-3R-1, 94–99	Ol gabbro, am, opx	2	48.71	75.24	67.49	63.76	49.99	74.23	
	Gabbronorite, zr	3	38.15	67.1	69.57		35.11	65.45	
921B-3R-1, 134–137	Ol gabbro, am, opx	0	54.89	77.18		70.15	55.54	78.01	71.93
921C-2R-1, 70–78	Ol gabbro, am	2	65.12	81.15		73.89	65.17		
	Ol gabbro, am, opx	3	65.24	82.53		77.01	65.75	85.41	79.29
921E-1R-1, 16–23	Ol gabbronorite, am, ox	1	55.26	78.26	72.49	63.53			
921E-2R-2, 54–60	Ol gabbro, am	1	56.05	80.29		65.37			
	Gabbronorite, ox, ap, am	4	38.59	65.78	53.88		35.96		59.18
921E-2R-2, 78–81	Ol gabbro, am, ox	1	57.6	79.68		65.62	56.74		
921E-3R-1, 3–9	Gabbronorite, ox, am, ap	3	58.18	66.22	62.06		39.88	65.99	61.18
921E-3R-1, 25–30	Ol gabbro, opx, ox	1	47.49	71.06	65.18	56.29	52.79		
	Leuc. segr., qz	0	26.56						
921E-3R-1, 37–41	Gabbronorite, am	3	42.03	64.67	56.57	38.5		66.46	
	Gabbronorite, am, ox	1	38.3	65.31	54.06	40.16			
	Leuc. segr.	0	26.74						
921E-7R-1, 25–29	Leuc. segr., qz, ap, zr	0	28.67	64.42					
921E-7R-2, 70–75	Ol gabbro, poik. cpx, am	0	69.08	85.17		78.06			
	Gabbronorite, ox	4	64.12	68.68	64.42		31.1	67.69	60.96
	Leuc. segr., zr	0	24.66						
921E-7R-2, 94–100	Gabbro, poik. cpx	0	65.23	84.87					
	Leuc. segr., qz, zr, sph	0	28.58						
922A-2R-2, 56–62	Ol gabbro, poik. cpx, opx	0	76.5	88.44	84.24	84.78			
	Gabbronorite myl, am	4	45.46	86.05	82.25		45.99	86.95	
922A-2R-2, 106–119	Troctolite, am	3	75.76			79.525	72.5		
	Norite, ox, ap	4	43.7		62.515		45.5		64.84
922A-2R-2, 123–128	Troctolite, poik. cpx, am	0	76.19	86.19			83.13		
	Gabbronorite myl, am	4	45.88	75.28	69.03		46.77	76.58	68.45
922A-2R-6, 18–25	Troctolite, poik. cpx, opx, am	1	69.6	86.92		79.08	70.08		83.66
	Gabbronorite, ox, am	3	71.14	72.29	67.33		58.9	77.36	
	Leuc. segr., ap, zr, am	0	36.09	64.32					
922A-3R-1, 63–66	Troctolite, poik. cpx, am, chr.	1	77.38	87.42		77.18	81.64		
	Gabbronorite, ol, am, ox	4	76.97	69.95	65.01	80.14	63.46		71.05
922B-1W-1, 109–115	Ol gabbro, poik. cpx, am	1	75.16	86.06		75.75	74.07		
	Troctolite, opx, am	4	75.24			83.89	73.07		78.15
	Gabbronorite, am, ox	3	56.09	76.65	64.44		57.82		73.43
922B-4R-1, 59–63	Altered gabbro, am	1	68.52						
	Altered, zr, am	4					39.64		
922B-4R-1, 67–74	Gabbro, poik. cpx	1	72.51	83.7					
	Gabbro, am, ap, zr	4	39.95	68.34			33.97		
	Leuc. segr., zr, am	0	33.2						
923A-2R-1, 13–16	Gabbronorite, ox, am	3	46.68	73	70.73		48.32	75.11	68.32
	Ol microgabbro, am	3	52.04	75.5		65.65			
923A-2R-2, 30–33	Gabbro, ox, am, ol, opx	0	49.085	73.65		61.72	48.91	66.59	
	Gabbronorite, ox	3	47.32	67.12	65.63		46.67		
	Gabbronorite, ox, am, ol, biot.	4		75.79	68.23		57.28	75.24	67.65
923A-3R-2, 51–57	Gabbro	2	56.41	73.54			54.28		
	Norite, ox, am, ap	4			65.51		48.62		
	Leuc. segr., ap, ox, am	0	46.09						
923A-8R-1, 31–46	Troctolite	0	71.39	81.61		75.18			
	Microgabbro	0	70.75	80.26					
	Gabbro	0	60.16	80.2					
923A-11R-1, 95–101	Ol gabbro, am	2	57.41	76.515		67.92			
	Gabbronorite	4		76.26	71.91		55.34		72.05
923A-12R-2, 26–31	Ol gabbro, am, opx	0	58.42	81.57	75.26	74.66			
	Microgabbronorite, am, ox	1	56.11	78.11	73.83				
923A-13R-1, 124–128	Ol gabbro, poik. cpx, opx, am	2	64.31	80.73	76.46	69.52	58.43		
	Gabbronorite, am	4			69.09		55.14	75.29	69.38
923A-13R-1, 136–142	Gabbronorite, ox, am	3	62.28	78.32	71.72		54.52	76.97	70.31
	Gabbro, opx, ol, am	4		76.41		68.62	57.11	77.33	73.91
923A-15R-2, 0–6	Ol gabbro, poik. cpx, am	1	60.58	75.32		68.03			
	Gabbro, ox, am, ap	4		73.57			47.76		
923A-16R-4, 6–12	Gabbro, poik. cpx, am	0	50.88	69.94					
	Gabbro	3	39.51	69.58			48.44	73.61	
	Leuc. segr., ap, sph, am	0	22.99						
923A-16R-4, 85–89	Ol gabbro	2	56.74	78.11		66.08	54.95		
	Leuc. segr., qz, ap, zr, am, ox	0	18.73	66.86					

Notes: See Tables 4, 5, and 6 for selected analyses. Text. type = textural type; Pl = plagioclase; Cpx = clinopyroxene; Opx = orthopyroxene; Ol = olivine; Ol gabbro = olivine gabbro; Leuc. segr. = leucocratic segregation; myl = mylonite; poik. cpx = poikilitic clinopyroxene; ox = iron titanium oxide; am = amphibole; zr = zircon; ap = apatite; qz = quartz; chr. = ferrichromite; biot. = biotite; sph = sphene; (R) = recrystallized.

that crystallized from the gabbronoritic parent melt would subsequently have been 100% recrystallized. In order to plot near the tholeiitic differentiation trend of Figure 6, this plagioclase should have had An contents between 35% and 50%. The most sodium-rich neoblasts have significantly lower An contents, similar to An contents in tablet-shaped plagioclase from the leucocratic segregations. We propose that this results from interactions between the deforming gabbronorite and patches of sodium- and silica-rich residual melt that later crystallized the leucocratic segregations. These interactions could have involved subsolidus reequilibration of plagioclase neoblasts and porphyroclasts with the melt patches and also crystallization of progressively less anorthitic igneous plagioclase from these melt patches before the end of ductile deformation.

Orthopyroxene in the gabbronorite in Sample 153-921E-7R-2, 70–75 cm, occurs as small euhedral grains (Fig. 5E), as even smaller and anhedral grains near olivine xenocrysts, and as polygonal neo-

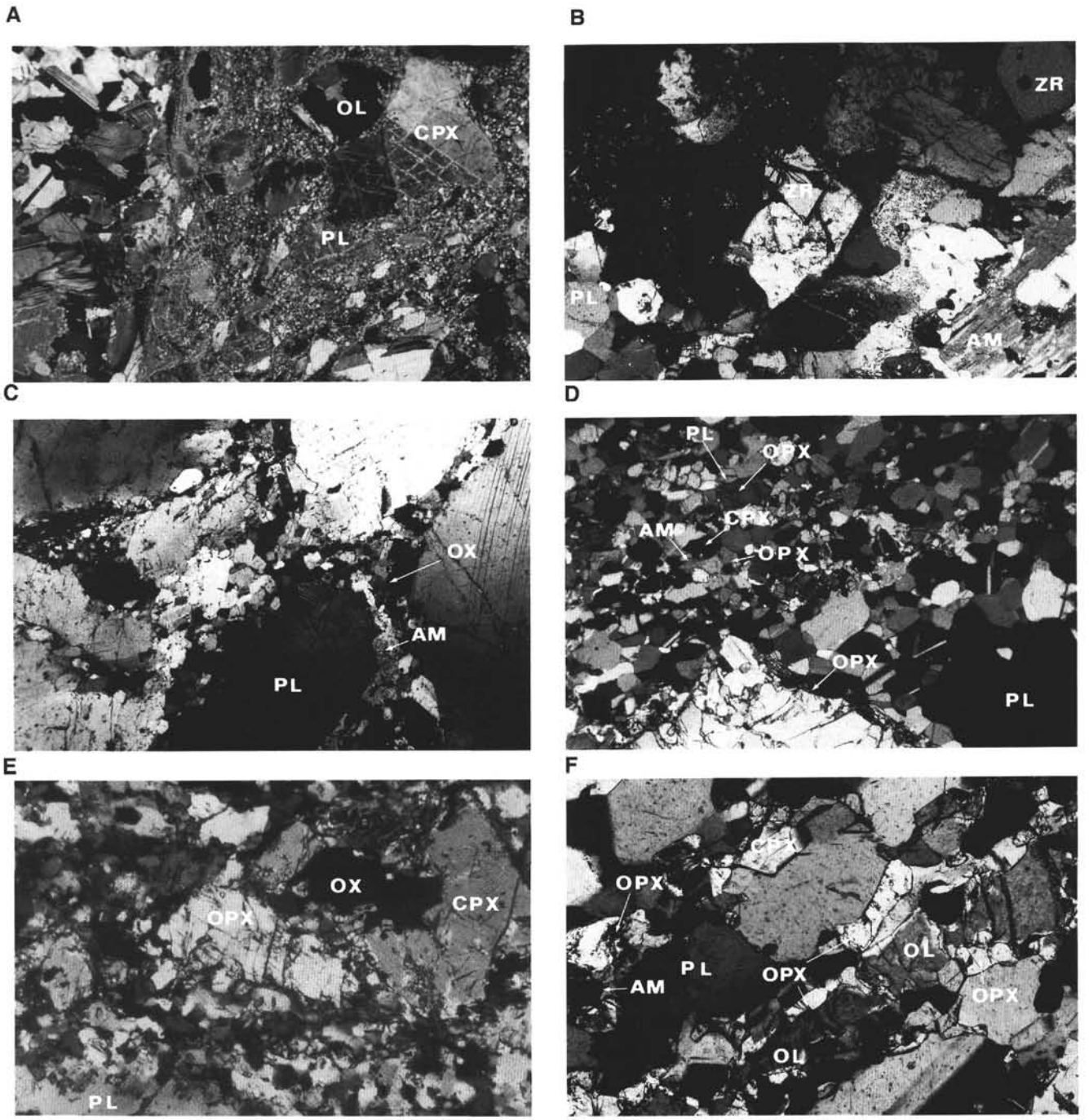

Figure 5. Photomicrographs (crossed nicols). Abbreviations as in Table 3. **A.** Sample 153-921E-7R-2, 70–75 cm. Mylonitic gabbronorite in medium-grained, undeformed olivine gabbro. This shear zone is fan-shaped and very fine-grained. It contains olivine, plagioclase, and clinopyroxene xenocrysts of the undeformed gabbro host. Length of view is 2.4 cm. **B.** Sample 153-923A-16R-4, 85–89 cm. Tablet-shaped plagioclase, euhedral zircon, and interstitial quartz form undeformed leucocratic segregation in deformed olivine gabbro (polygonal recrystallized plagioclase visible in lower left corner). Length of view is 3.2 mm. **C.** Sample 153-921E-3R-1, 25–30 cm. Plagioclase-rich domain in moderately deformed olivine gabbro. Plagioclase porphyroclasts are rimmed by fine-grained, polygonal, plagioclase neoblasts and also by undeformed rectangular-to-square, small, plagioclase grains that form leucocratic segregations with minor interstitial amphibole and oxides. Length of view is 3.2 mm. **D.** Sample 153-923A-13R-1, 124–128 cm. Contact between weakly deformed olivine gabbro and an extensively recrystallized gabbronorite with oval-shaped pyroxenes, and aggregates of polygonal plagioclase, pyroxene, and minor brown amphibole neoblasts (core photograph in Fig. 2C). Length of view is 3.2 mm. **E.** Sample 153-921E-7R-2, 70–75 cm. Detail of mylonitic gabbronorite (see Fig. 5A) with a square igneous clinopyroxene, a rectangular igneous orthopyroxene, a grain of iron-titanium oxide in finely recrystallized plagioclase. Part of a ribbon-shaped plagioclase porphyroclast is visible in lower left corner. Length of view is 2 mm. **F.** Sample 153-923A-13R-1, 136–142 cm. Foliated olivine gabbro in shear zone, pictured in Figure 2C, contains ribbon-shaped, partly recrystallized, olivine relics coated by polygonal grains of orthopyroxene. Recrystallized aggregate near olivine includes polygonal plagioclase, orthopyroxene, clinopyroxene, and minor brown amphibole. Length of view is 1.2 mm.

Table 4. Selected microprobe analyses of clinopyroxene in gabbroic rocks listed in Table 3.

Sample no:	921E-7R-1, 25–29 cm	921E-2R-2, 54–60 cm			921E-7R-2, 70–75 cm						923A-2R-1, 13–16 cm			923A-12R-2, 26–31 cm		921E-3R-1, 37–41 cm		
Text. type:	0	1	1	4	0	0	4	4	4	4	3	3	3	0	0	2	2	1
	P	P	P	P	P	P	P	P	Prim	R	P	R	P	Int.	P	P	R	P
Na_2O	0.45	0.34	0.39	0.46	0.39	0.43	0.35	0.35	0.43	0.43	0.47	0.41	0.44	0.38	0.42	0.43	0.34	0.41
Cr_2O_3	0.02	0.09	0.14	0	1.08	0.8	0.98	0.86	0.08	0.02	0.02	0.09	0.12	0.11	0.03	0	0	0.01
MgO	11.81	17.06	15.41	12.64	16.26	18.64	16.07	16.96	13.7	13.28	14.06	14.58	15.22	16.05	14.92	12.92	12.93	12.65
Al_2O_3	0.33	2.66	2.28	1.7	4.02	2.92	3.83	3.54	0.72	0.76	2.49	2.26	2.4	2.3	2.42	1.94	1.41	1.87
SiO_2	52.85	52.56	51.77	51.27	51.39	52.69	51.38	51.78	52.74	52.34	50.98	51.46	51.73	52.13	51.51	51.7	52.25	51.9
CaO	21.81	20.62	20.29	20.13	21.33	17.23	22.28	21.08	21.01	20.93	20.85	21.15	20.55	21.88	21.54	19	20.04	19.28
TiO_2	0.09	0.58	0.58	0.64	0.44	0.33	0.45	0.41	0.19	0.22	1.03	0.6	0.85	0.75	1.08	0.52	0.37	0.62
MnO	0.54	0.2	0.27	0.46	0.14	0.11	0.1	0.09	0.34	0.4	0.3	0.23	0.23	0.16	0.25	0.44	0.42	0.44
FeO	11.85	5.84	8.38	12.77	4.33	6.67	3.71	4.4	10.49	11.3	9.24	8.62	7.97	5.83	7.5	12.79	11.57	11.8
NiO	0.01	0.01	0	0.05	0.02	0.03	0.03	0.02	0.01	0.03	0.04	0.04	0	0	0.04	0.01	0.01	0.01
CalcTotal	99.76	99.96	99.52	100.11	99.4	99.86	99.17	99.49	99.72	99.7	99.48	99.43	99.5	99.58	99.7	99.75	99.34	99.01
Mg#	63.985	83.887	76.626	63.832	86.996	83.28	88.538	87.295	69.954	67.697	73.056	75.108	77.285	83.065	78.01	64.299	66.57	65.657

Notes: Text. type = textural type; P = porphyroclast core; Prim = porphyroclast rim; R = recrystallized; Int. = interstitial. CalcTotal = calculated total.

Table 4 (continued).

Sample no:	921E-2R-2, 78–81 cm		921E-3R-1, 25–30 cm	921E-1R-1, 16–23 cm	923A-13R-1, 124–128 cm					923A-13R-1, 136–142 cm						923A-2R-2, 30–33 cm				
Text. type:	1	1	1	1	2	2	2	4	4	3	3	3	4	4	4	1	1	4	4	2
	P	P	P	P	P	R	P	R	R	P	P	R	P	R	R	P	P	P	R	P
Na_2O	0.42	0.31	0.48	0.38	0.45	0.39	0.36	0.41	0.41	0.4	0.39	0.42	0.43	0.39	0.4	0.42	0.45	0.42	0.39	0.46
Cr_2O_3	0.09	0.08	0.05	0.04	0.7	0.64	0.35	0.46	0.08	0.02	0.18	0.24	0.21	0.08	0.12	0.05	0.02	0.28	0.08	0.04
MgO	14.72	15.97	14.54	14.62	14.77	15.41	16.4	14.95	14.45	15.74	16.17	14.92	14.85	14.83	15.16	14.46	14.19	14.81	14.64	14.35
Al_2O_3	2.67	2.28	2.9	2.62	3.67	3.68	2.97	2.48	2.02	2.4	2.95	2.83	2.61	2.08	2.12	2.44	2.26	2.7	2.21	2.5
SiO_2	52.25	52.55	51.96	51.65	51.57	52.91	52.75	52.9	53.13	51.56	52.43	51.82	52.06	52.6	52.42	52.14	52.09	52.55	51.85	51.16
CaO	20.69	21.85	20.88	20.8	20.47	21.72	20.08	20.94	20.41	17.25	20.79	20.66	21.02	20.68	21.36	20.62	20.71	20.96	21.21	20.74
TiO_2	0.96	0.56	0.98	0.72	0.63	0.5	0.65	0.55	0.59	0.96	0.54	0.88	0.85	0.67	0.64	0.76	0.77	0.96	0.62	0.87
MnO	0.25	0.12	0.19	0.22	0.18	0.14	0.19	0.21	0.31	0.32	0.2	0.28	0.27	0.22	0.17	0.27	0.31	0.28	0.26	0.29
FeO	8.53	6.05	8.05	7.38	7.17	5.13	5.9	7.7	9.32	10.97	5.95	7.96	7.99	8.64	7.32	8.77	10.17	8.43	8.02	8.91
NiO	0	0.01	0	0.01	0	0	0.06	0.03	0.05	0.000	0.000	0.000	0.04	0.04	0.02	0	0	0	0	0.01
CalcTotal	100.59	99.78	100.03	98.43	99.6	100.53	99.71	100.63	100.78	99.63	99.61	100.01	100.34	100.21	99.74	99.91	100.96	101.38	99.29	99.35
Mg#	75.459	82.47	76.305	77.933	78.595	84.265	83.217	77.578	73.427	71.891	82.9	76.975	76.821	75.37	78.678	74.625	71.33	75.795	76.5	74.159

Table 4 (continued).

Sample no:	921E-7R-2, 94–100 cm	921E-3R-1, 3–9 cm		923A-16R-4, 85–89 cm			923A-11R-1, 95–101 cm		923A-3R-2, 51–57 cm		923A-8R-1, 31–46 cm					923A-15R-2, 0–6 cm	
Text. type:	0	3	3	2	2	0	2	4	2	2	0	0	0	0	0	1	4
	P	P	R	P	P	P	P	P	P	P	P	P	P	P	P	P	P
Na_2O	0.47	0.41	0.36	0.38	0.37	0.45	0.53	0.41	0.4	0.4	0.43	0.41	0.34	0.42	0.45	0.38	0.42
Cr_2O_3	0.37	0.02	0	0.09	0.11	0.01	0.05	0.08	0.06	0.04	0.16	0.17	0.12	0.05	0.11	0.36	0.08
MgO	15.96	12.76	13.18	16.01	16.33	12.71	14.1	14.3	15.07	14.23	15.39	15.92	16.48	15.1	15.22	14.47	14.01
Al_2O_3	2.42	1.83	1.44	2.48	2.88	0.62	2.78	2.62	2.08	2.43	3.1	3.45	3.01	2.84	3.22	3.58	1.58
SiO_2	52.74	51.08	52.11	52.16	51.95	52.36	51.41	51.69	52.44	51.68	52.66	50.39	53.72	52.47	51.17	51.01	52.48
CaO	21.72	18.95	19.34	19.14	20.09	20.55	21.02	21.48	20.61	19.98	21.68	20.25	20.24	21.39	22.19	20.51	20.87
TiO_2	0.69	0.63	0.38	0.81	0.6	0.18	1.01	0.77	0.55	0.73	1.06	1.12	0.7	1.04	1.2	0.69	0.45
MnO	0.15	0.42	0.43	0.22	0.23	0.46	0	0.26	0.23	0.31	0.14	0.2	0.19	0.22	0.19	0.21	0.25
FeO	4.86	13.13	12.1	8.67	6.36	11.9	8.49	7.84	8.11	9.97	5.84	7.03	6.45	7.2	6.11	8.11	9.74
NiO	0.01	0	0.01	0.07	0.03	0.02	0.02	0	0	0.02	0.01	0.02	0.07	0.01	0.05	0.02	0
CalcTotal	99.42	99.24	99.37	100.04	98.95	99.28	99.41	99.47	99.55	99.78	100.46	98.96	101.33	100.74	99.91	99.36	99.89
Mg#	85.406	63.412	66.021	76.7	82.062	65.559	74.752	76.48	76.81	71.78	82.45	80.138	81.997	78.884	81.615	76.097	71.945

Table 4 (continued).

Sample no:	923A-16R-4, 6–12 cm		922A-2R-6, 18–25 cm						922A-3R-1, 63–66 cm		922B-4R-1, 67–74 cm		922A-2R-2, 123–128 cm			922A-2R-2, 56–62 cm		
Text. type:	0	3	1	3	3	0	3	1	4	1	1	4	4	4	0	4	4	0
	P	P	P	P	R	P	P	P	P	P	P	P	P	R	P	R	P	P
Na_2O	0.44	0.49	0.43	0.4	0.31	0.4	0.35	0.3	0.4	0.67	0.57	0.42	0.41	0.37	0.4	0.31	0.35	0.49
Cr_2O_3	0.08	0.04	0.15	0.47	0.17	0.000	0.02	1.01	0.01	0.39	0.05	0.02	0.07	0.03	0.38	0.04	0.06	0.46
MgO	13.47	13.06	13.8	13.44	14.69	12.83	13.78	17.87	14.21	16.64	15.66	13.49	14.62	14.8	15.97	16.54	16.53	16.15
Al_2O_3	2.18	2.09	2.49	2.44	1.000	1.64	1.43	3.19	1.5	3.39	3.33	1.05	1.95	1.35	2.95	1.26	1.39	3.41
SiO_2	50.85	50.54	51.6	51.76	53.24	51.73	52.5	52.75	51.66	50.85	52.3	52.84	51.79	52.67	51.57	53.19	52.63	50.91
CaO	20.97	20.58	20.93	21.45	21.49	19.39	20.15	20.23	20.52	21.52	21.34	20.26	19.93	21.88	22.77	22.77	22.17	21.9
TiO_2	0.74	0.74	0.78	0.65	0.24	0.54	0.41	0.41	0.53	1.31	1.01	0.29	0.74	0.41	1.23	0.59	0.64	1.49
MnO	0.36	0.39	0.32	0.34	0.37	0.48	0.31	0.12	0.43	0.11	0.19	0.52	0.3	0.3	0.16	0.12	0.16	0.15
FeO	10.02	10.59	9.16	8.93	8.32	12.69	10.7	4.19	10.23	3.71	5.43	11.48	9.23	8.07	4.12	4.43	4.78	3.88
NiO	0.02	0	0.000	0.000	0.02	0.01	0.03	0.02	0.03	0	0.05	0.03	0.07	0.01	0.04	0.02	0.06	0.06
CalcTotal	99.14	98.5	99.68	99.9	99.85	99.71	99.68	100.09	99.53	98.59	99.93	100.39	99.12	99.89	99.59	99.28	98.77	98.88
Mg#	70.571	68.738	72.869	72.839	75.879	64.322	69.655	88.374	71.219	88.887	83.706	67.692	73.848	76.578	87.364	86.953	86.05	88.123

Table 4 (continued).

Sample no:	921B-3R-1, 33–36 cm	921B-3R-1, 94–99 cm			922B-1W-1, 109–115 cm			921B-3R-1, 134–137 cm		921B-3R-1, 71–79 cm					921C-2R-1, 70–78 cm		
Text. type:	3	2	2	3	3	1	1	0	0	3	3	3	3	3	3	3	2
	P	P	R	P	P	P	P	P	R vein	P	P	R	P	R	R	P	P
Na_2O	0.45	0.42	0.33	0.37	0.36	0.47	0.36	0.46	0.45	0.36	0.4	0.36	0.44	0.36	0.34	0.46	0.38
Cr_2O_3	0	0.07	0.02	0.02	0.000	1.05	0.43	0.05	0.03	0.13	0.21	0.09	0	0.03	0.35	0.59	0.28
MgO	13.34	14.58	14.12	13.19	15.4	15.32	15.87	14.95	14.85	14.45	15.23	14.18	12.85	12.94	15.66	15.42	15.4
Al_2O_3	1.96	2.48	1.36	1.04	1.87	3.54	2.82	2.57	2.25	2.55	3	2.44	2.09	1.78	1.96	3.28	2.26
SiO_2	51.83	51.93	52.22	52.28	51.68	50.93	51.92	52.36	52.55	51.29	51.98	51.53	51.22	51.4	52.67	52.23	52.51
CaO	19.92	20.82	21.15	20.48	19.85	21.72	22.85	21.03	21.38	20.47	21.6	20.53	20.2	20.07	22.22	21.25	21.73
TiO_2	0.61	0.82	0.49	0.37	0.62	0.88	1.04	0.75	0.72	0.8	0.6	0.82	0.75	0.5	0.55	0.47	0.44
MnO	0.32	0.23	0.3	0.38	0.31	0.13	0.12	0.23	0.22	0.24	0.2	0.22	0.4	0.39	0.17	0.21	0.17
FeO	11.78	8.2	9.34	11.67	8.36	4.54	4.13	7.81	7.65	9.14	6.34	8.61	11.34	11.69	4.76	5.57	5.88
NiO	0	0.01	0.03	0.08	0.000	0.05	0.01	0.02	0.02	0	0.04	0	0.04	0.01	0.01	0	0.03
CalcTotal	100.21	99.55	99.37	99.88	98.47	98.64	99.56	100.26	100.15	99.43	99.6	98.78	99.32	99.18	98.71	99.48	99.09
Mg#	66.867	76.027	72.933	66.83	76.652	85.742	87.271	77.346	77.579	73.81	81.067	74.597	66.891	66.355	85.415	83.156	82.356

Table 5. Selected microprobe analyses of plagioclase in gabbroic rocks listed in Table 3.

Sample no:	921E-7R-1, 25-29 cm	921E-2R-2, 56–60 cm				921E-7R-2, 70–75 cm						923A-2R-1, 13–16 cm			923A-12R-2, 26–31 cm	
Text. type:	0	1	1	4	4	0	0	4	4	4	0	3	3	3	0	0
	P	P	P	P	R	P	P	P	R	R	P	P	R	P	P	P
Na_2O	8.26	5.86	4.51	7.11	7.68	3.57	2.68	3.44	5.31	8.53	8.65	6.08	6.08	5.58	4.64	5.04
MgO	0	0.03	0.01	0.03	0.01	0.02	0.01	0.01	0	0	0.01	0.04	0.04	0.02	0.04	0.03
Al_2O_3	24.03	27.88	30.19	26.21	25.35	30.71	32.13	30.71	28.33	23.92	23.04	27.35	27.46	28.36	29.74	29.01
SiO_2	62.07	56.1	53.02	58.74	60.45	50.91	49.02	50.9	54.92	61.46	62.74	56.59	56.55	55.35	52.98	53.86
CaO	5.72	10.49	12.75	8.17	7.18	14.16	15.58	14.24	11.01	5.7	4.88	9.83	10.14	10.84	12.35	11.73
TiO_2	0.02	0.1	0.08	0.04	0.03	0.06	0.01	0.04	0.01	0	0.02	0.05	0.04	0.04	0.06	0.11
FeO	0.22	0.22	0.22	0.16	0.16	0.19	0.29	0.16	0.15	0.19	0.17	0.32	0.3	0.27	0.31	0.28
K_2O	0.29	0.08	0.04	0.12	0.11	0.02	0.02	0.04	0.05	0.13	0.25	0.08	0.1	0.05	0.02	0.05
CalcTotal	100.65	100.77	100.84	100.57	100.98	99.75	99.82	99.55	99.8	99.94	99.77	100.34	100.72	100.53	100.12	100.12
Mg#	2.384	18.018	9.73	24.818	10.138	17.491	6.804	11.728	0	4.436	7.868	16.575	20.459	10.622	17.383	17.622
Albite	71.139	50.03	38.946	60.751	65.555	31.28	23.73	30.351	46.497	72.506	75.139	52.55	51.748	48.11	40.424	43.614
Anorthite	27.222	49.515	60.798	38.591	33.849	68.576	76.177	69.434	53.232	26.751	23.443	46.983	47.698	51.595	59.473	56.073
Orthoclase	1.639	0.455	0.256	0.658	0.595	0.144	0.093	0.215	0.271	0.744	1.418	0.467	0.554	0.295	0.103	0.313

Notes: Text. type = textural type; P = porphyroclast core; Prim = porphyroclast rim; R = recrystallized.

Table 5 (continued).

Sample no:	921E-3R-1, 37–41 cm							921E-2R-2, 78–81 cm			921E-3R-1, 25-30 cm				921E-1R-1, 16–23 cm		923A-13R-1, 124–128 cm			
Text. type:	2	2	2	2	0	1	1	1	1	1	1	1	0	0	1	1	2	2	4	4
	P	P	R	P	P	P	R	P	P	R	P	P	P	P	P	P	P	R	R	R
Na_2O	4.31	6.92	6.84	6.83	8.27	6.91	6.85	4.7	5.36	4.67	5.32	6.43	7.78	9.72	4.81	5.51	3.98	4.63	3.75	5.39
MgO	0.01	0.02	0.01	0.01	0	0.02	0.02	0.03	0.02	0.02	0.02	0.02	0.01	0	0.04	0	0.02	0.02	0	0.02
Al_2O_3	30.12	26.11	26.17	26.24	24.14	25.88	26.47	29.53	28.64	29.36	28.89	27.09	24.63	21.91	29.47	28.52	30.63	29.65	30.99	28.94
SiO_2	53.54	58.86	58.95	58.98	62.62	58.69	58.91	53.94	55.31	54.33	55.5	58.14	61.18	66.02	54.35	55.57	52.18	53.98	51.96	55.52
CaO	12.14	7.7	7.89	7.88	5.4	7.7	7.98	11.81	10.62	11.8	10.76	8.74	6.06	2.73	11.34	10.26	13.47	12.16	13.59	11.06
TiO_2	0.06	0.05	0.02	0.02	0	0.04	0.02	0.08	0.09	0.06	0.07	0.08	0.01	0.01	0.06	0.02	0.05	0.04	0.04	0.04
FeO	0.23	0.19	0.23	0.23	0.15	0.26	0.2	0.25	0.19	0.23	0.2	0.29	0.14	0.14	0.17	0.14	0.18	0.28	0.23	0.16
K_2O	0.08	0.16	0.17	0.17	0.28	0.09	0.08	0.09	0.06	0.05	0.07	0.13	0.16	0.31	0.07	0.08	0.02	0.05	0.03	0.05
CalcTotal	100.5	100.04	100.34	100.37	100.87	99.62	100.53	100.41	100.32	100.54	100.86	100.99	100	100.87	100.33	100.14	100.56	100.82	100.66	101.22
Mg#	9.3	13.818	9.153	7.193	3.465	14.537	13.649	17.564	15.661	14.354	15.259	12.462	8.292	5.829	26.618	6.026	18.054	12.285	3.7	22.22
Albite	38.914	61.313	60.455	60.488	72.296	61.59	60.561	41.636	47.554	41.601	47.037	56.708	69.26	85.02	43.234	49.053	34.815	40.676	33.225	46.73
Anorthite	60.622	37.725	38.538	38.544	26.104	37.906	38.997	57.839	52.096	58.095	52.573	42.549	29.786	13.214	56.34	50.508	65.087	59.041	66.611	53.007
Orthoclase	0.464	0.962	1.007	0.967	1.6	0.504	0.442	0.525	0.351	0.305	0.39	0.742	0.954	1.767	0.426	0.439	0.098	0.283	0.163	0.262

Table 5 (continued).

Sample no:	923A-13R-1, 136–142 cm			923A-2R-2, 30–33 cm							921E-7R-2, 94–100 cm					921E-3R-1, 3–9 cm		
Text. type:	3	3	4	1	3	3	4	4	2	2	0	0	0	0	0	3	3	3
	P	R	R	P	P	R	R	R	P	R	P	P	P	P	P rim	P	R	R
Na_2O	4.24	5.23	4.9	5.92	6.03	6.14	3.67	5.53	5.68	5.78	3.88	7.11	7.59	8.39	10.03	4.23	7.06	6.79
MgO	0.03	0.01	0.01	0.04	0.02	0.01	0.02	0.02	0.03	0.03	0	0	0.01	0	0	0.01	0.01	0
Al_2O_3	30.08	28.84	29.26	27.75	27.93	27.81	30.96	28.6	27.53	27.76	31.23	26.18	25.17	24.2	21.54	30.3	26.04	26.69
SiO_2	53.29	55.34	54.57	56.03	56.66	56.55	50.9	55.57	55.67	55.54	52.39	58.82	60.85	62.07	65.87	52.61	59.01	58.41
CaO	12.77	10.92	11.63	10.18	9.95	9.79	13.77	10.77	10.06	10.11	13.33	7.55	6.5	5.29	2.37	12.35	7.44	8.11
TiO_2	0.05	0.05	0.03	0.12	0.09	0.04	0.05	0	0.04	0.04	0.06	0.03	0.04	0.02	0.01	0.07	0.02	0.04
FeO	0.25	0.25	0.18	0.37	0.25	0.3	0.29	0.18	0.24	0.25	0.2	0.19	0.27	0.29	0.17	0.26	0.23	0.52
K_2O	0.05	0.1	0.06	0.08	0.11	0.07	0.02	0.05	0.08	0.06	0.02	0.08	0.31	0.38	0.45	0.05	0.11	0.1
CalcTotal	100.76	100.8	100.65	100.6	101.05	100.74	99.7	100.8	99.35	99.58	101.11	99.98	100.75	100.68	100.44	99.89	99.94	100.67
Mg#	16.144	8.452	13.06	16.458	11.295	7.238	12.538	16.305	16.763	17.564	4.246	0	7.242	3.012	0	4.596	8.343	1.024
Albite	37.418	46.177	43.111	51.044	51.988	52.92	32.511	48.021	50.306	50.707	34.473	62.698	66.694	72.551	86.23	38.165	62.793	59.89
Anorthite	62.28	53.254	56.559	48.479	47.399	46.671	67.343	51.682	49.21	48.965	65.41	36.832	31.526	25.304	11.236	61.532	36.592	39.541
Orthoclase	0.302	0.569	0.33	0.476	0.613	0.409	0.146	0.297	0.483	0.329	0.117	0.47	1.78	2.146	2.534	0.302	0.615	0.569

Table 5 (continued).

Sample no:	923A-16R-4, 85–89 cm				923A-11R-1, 95–101 cm			923A-3R-2, 51–57 cm				923A-8R-1, 31–46 cm					
Text. type:	2	2	0	0	2	2	4	2	2	4	0	0	0	0	0	0	0
	P	R	P	P	P	P	R	P	R	R	P	P	P	P	P	P	P
Na_2O	4.71	5.11	10.47	7.34	4.55	4.83	4.79	4.81	5.12	5.89	6.14	2.6	3.76	3.11	4.01	3.46	5.1
MgO	0.03	0.01	0.000	0.02	0.01	0.01	0	0.02	0.02	0.02	0.02	0.02	0.04	0.03	0.03	0.03	0.03
Al_2O_3	29.33	28.8	21.33	25.28	29.16	29.61	29.29	28.76	28.39	27.37	27.18	32.39	30.55	31.78	30.64	31.06	28.88
SiO_2	53.74	54.7	66.07	59.03	53.14	53.93	53.65	53.38	54.39	56.15	56.27	48.89	51.42	49.62	51.77	51.19	55.03
CaO	11.86	11.15	2.21	7.19	12.21	11.94	11.53	11.82	11.06	9.9	9.58	15.67	13.71	15.21	13.57	14.11	11.41
TiO_2	0.08	0.05	0.01	0.04	0.06	0.06	0.04	0.07	0.03	0.04	0.04	0.04	0.07	0.06	0.08	0.04	0.09
FeO	0.27	0.21	0.01	0.27	0.3	0.24	0.21	0.31	0.21	0.31	0.31	0.28	0.25	0.3	0.29	0.35	0.29
K_2O	0.06	0.07	0.06	0.26	0.05	0.06	0.04	0.08	0.04	0.08	0.09	0.03	0.05	0.04	0.04	0.02	0.06
CalcTotal	100.14	100.11	100.19	99.47	99.51	100.74	99.56	99.28	99.26	99.78	99.62	99.96	99.86	100.16	100.43	100.32	100.92
Mg#	15.225	11.295	0.000	13.183	7.238	8.907	2.472	9.352	12.507	11.198	9.463	12.975	24.515	13.786	16.629	14.118	16.961
Albite	41.65	45.139	89.24	63.889	40.149	42.114	42.806	42.237	45.49	51.622	53.418	23.055	33.084	26.93	34.735	30.688	44.579
Anorthite	57.977	54.454	10.418	34.598	59.566	57.559	56.958	57.284	54.282	47.94	46.09	76.746	66.615	72.865	65.019	69.207	55.082
Orthoclase	0.373	0.407	0.342	1.513	0.285	0.327	0.235	0.479	0.228	0.438	0.493	0.198	0.301	0.205	0.245	0.105	0.339

Table 5 (continued).

Sample no:	923A-15R-2, 0–6 cm				922A-2R-2, 106–111 cm				922A-2R-2, 123–128 cm				922B-4R-1, 59–63 cm		
Text. type:	1	1	4	4	3	3	4	4	0	0	4	4	1	1	4
	P	P	R	R	P	R	P	R	P	P	P	R	P	R	P
Na_2O	4.64	2.95	5.16	6.72	2.92	2.89	6.5	6.51	3.15	2.34	6.12	6	3.43	3.63	6.76
MgO	0.02	0.01	0.02	0.01	0.03	0.03	0.01	0.01	0.03	0.03	0.01	0.01	0.02	0.02	0.01
Al_2O_3	29.62	31.89	28.83	26.64	31.95	31.76	26.22	26.42	31.57	32.84	27.46	27.46	31.82	31.59	26.29
SiO_2	53.24	49.7	54.53	58.19	49.11	49.67	56.73	56.57	49.76	48.15	56.86	56.64	51.66	51.79	58.41
CaO	12.29	15	11.28	8.58	15.51	15.38	9.17	9.22	14.67	16.16	9.48	9.76	14.34	13.94	8.19
TiO_2	0.06	0.04	0.03	0.05	0.06	0.01	0.05	0.1	0.08	0.04	0.02	0.02	0.08	0.04	0.04
FeO	0.3	0.35	0.33	0.17	0.18	0.24	0.29	0.22	0.16	0.19	0.12	0.16	0.26	0.19	0.16
K_2O	0.08	0.03	0.1	0.1	0.02	0.06	0.11	0.12	0.01	0.03	0.14	0.12	0.05	0.02	0.02
CalcTotal	100.25	100	100.3	100.45	99.8	100.11	99.14	99.2	99.44	99.82	100.22	100.22	101.69	101.24	99.88
Mg#	10.718	6.26	9.777	6.952	21.474	16.589	7.376	8.717	27.13	20.47	12.481	11.601	10.403	14.448	9.968
Albite	40.419	26.227	45.022	58.287	25.362	25.32	55.863	55.703	27.969	20.724	53.432	52.338	30.083	32.012	59.847
Anorthite	59.117	73.598	54.393	41.142	74.506	74.34	43.51	43.643	71.955	79.078	45.763	46.996	69.617	67.854	40.049
Orthoclase	0.464	0.175	0.586	0.571	0.132	0.34	0.627	0.654	0.076	0.198	0.805	0.665	0.301	0.133	0.105

Table 5 (continued).

Sample no:	922A-2R-6, 18–25 cm															922A-3R-1, 63–66 cm				
Text. type:	1	1	1	3	3	3	0	0	3	3	3	1	1	1	1	1	1	4	4	4
	P	P	R	P	R	R	P	P	P	R	R	P	P	R	R	P	R	P	R	R
Na_2O	5.87	3.17	5.66	2.64	2.58	4.82	8.18	7.39	3.16	3.34	6.09	4.94	2.5	4.83	2.82	2.15	2.24	2.76	2.64	6.68
MgO	0.01	0.02	0.000	0.01	0.000	0.01	0.000	0.01	0.02	0.01	0.01	0.03	0.03	0.01	0.000	0.02	0.02	0.01	0.02	0.01
Al_2O_3	27.41	31.52	27.86	32.5	32.69	29.28	24.36	25.42	31.62	31.5	27.48	29.02	32.64	29.25	32.31	33.1	33.02	32.35	32.4	26.21
SiO_2	56.69	50.73	56.29	49.27	49.03	54.6	62.19	60.46	50.37	50.39	57.39	54.28	48.08	53.67	49.35	48.11	48.04	48.78	48.48	58.09
CaO	9.57	14.55	10.18	15.41	15.58	11.62	5.67	7.14	14.56	14.53	9.35	11.45	15.97	11.77	15.38	16.37	16.49	15.44	15.71	8.2
TiO_2	0.05	0.08	0.07	0.04	0.03	0.03	0.03	0.02	0.06	0.05	0.04	0.11	0.04	0.05	0.04	0.04	0.01	0.05	0.04	0.06
FeO	0.19	0.35	0.19	0.18	0.23	0.2	0.08	0.22	0.3	0.19	0.15	0.23	0.17	0.18	0.28	0.17	0.23	0.16	0.16	0.15
K_2O	0.15	0.04	0.12	0.02	0.03	0.05	0.05	0.24	0.02	0.03	0.1	0.08	0.03	0.05	0.02	0.02	0.02	0.01	0.01	0.12
CalcTotal	99.95	100.53	100.38	100.1	100.2	100.61	100.61	100.9	100.12	100.07	100.61	100.17	99.52	99.84	100.22	100.05	100.08	99.58	99.53	99.56
Mg#	10.871	8.376	0.000	10.569	2.234	5.929	4.071	5.391	9.231	8.703	13.305	17.832	21.57	11.635	3.085	17.421	15.356	7.955	22.11	7.541
Albite	52.148	28.208	49.813	23.621	23.041	42.778	72.098	64.293	28.19	29.294	53.77	43.655	22.057	42.489	24.858	19.183	19.695	24.425	23.314	59.126
Anorthite	46.998	71.552	49.509	76.237	76.783	56.954	27.629	34.326	71.663	70.532	45.654	55.891	77.763	57.216	75.014	80.688	80.189	75.529	76.604	40.157
Orthoclase	0.854	0.24	0.678	0.141	0.176	0.268	0.273	1.38	0.147	0.173	0.576	0.453	0.18	0.295	0.128	0.129	0.116	0.047	0.081	0.717

Table 5 (continued).

Sample no:	922B-4R-1, 67–74 cm					922A-2R-2, 56–62 cm			921B-3R-1, 33–36 cm		921B-3R-1, 94–99 cm				
Text. type:	1	1	4	4	0	4	4	0	3	3	2	2	2	3	3
	P	P	P	R	P	P	R	P	P	R	P	P	R	P	R
Na_2O	2.78	3.8	7.1	7.36	7.85	6.15	5.9	2.37	6.02	5.8	6.29	5.35	5.59	6.95	7.3
MgO	0.02	0.02	0	0.01	0	0.01	0.01	0.03	0.02	0.02	0.03	0.02	0.01	0.01	0.01
Al_2O_3	32.49	30.61	25.97	25.89	25.3	27.01	27.15	32.58	27.64	28.05	26.77	28.32	28.1	25.9	25.31
SiO_2	50	51.6	59.29	59.76	61.02	56.45	56.38	48.1	57.34	56.75	57.9	55.7	56.11	59.4	60.52
CaO	15.4	13.5	7.94	7.51	6.68	9.42	9.46	15.94	9.46	9.96	8.98	10.78	10.32	7.71	7.06
TiO_2	0.03	0.05	0.01	0.01	0	0.03	0.05	0.05	0.07	0.04	0.04	0.08	0.05	0.02	0.01
FeO	0.21	0.19	0.21	0.12	0.19	0.12	0.11	0.17	0.22	0.19	0.27	0.19	0.11	0.16	0.15
K_2O	0.02	0.03	0.18	0	0.04	0.15	0.16	0.04	0.1	0.08	0.11	0.08	0.1	0.12	0.17
CalcTotal	100.99	99.8	100.74	100.67	101.09	99.33	99.24	99.29	100.92	100.89	100.39	100.52	100.39	100.28	100.56
Mg#	12.611	13.818	1.669	10.782	4.549	9.712	11.958	24.366	15.649	15.87	16.635	14.646	19.273	7.193	13.618
Albite	24.602	33.666	61.187	63.957	67.902	53.694	52.529	21.138	53.217	51.05	55.544	47.064	49.204	61.579	64.559
Anorthite	75.305	66.153	37.809	36.043	31.898	45.467	46.534	78.65	46.19	48.481	43.812	52.449	50.228	37.745	34.469
Orthoclase	0.093	0.181	1.004	0	0.199	0.839	0.937	0.211	0.593	0.469	0.645	0.487	0.568	0.676	0.971

Table 5 (continued).

Sample no:	922B-1W-1, 109–115 cm											921B-3R-1, 134–137 cm	
Text. type:	1	1	1	3	3	3	3	4	4	4	4	0	0
	P	P	R	P	P	R	R	P	P	R	R	P	R vein
Na_2O	3.19	2.27	2.74	6.18	2.88	6.24	2.28	2.22	3.06	2.59	4.15	5.08	4.94
MgO	0.02	0.02	0.01	0.03	0.000	0.02	0.02	0.01	0.05	0.02	0.14	0.04	0.02
Al_2O_3	31.32	32.95	32.31	26.8	31.55	26.73	32.3	32.89	31.93	32.37	29.68	28.84	29.05
SiO_2	49.86	48	49.36	56.72	48.8	56.61	47.66	47.55	49.64	48.72	52.79	54.72	54.34
CaO	14.36	16.16	15.19	9.31	15.16	9.21	16.04	16.32	14.92	15.69	12.16	11.27	11.46
TiO_2	0.04	0.04	0.07	0.05	0.07	0.05	0.04	0.03	0.06	0.04	0.03	0.06	0.05
FeO	0.15	0.11	0.12	0.29	0.23	0.21	0.24	0.16	0.12	0.13	0.39	0.38	0.27
K_2O	0.04	0.02	0.03	0.11	0.02	0.12	0.03	0.03	0.05	0.04	0.05	0.05	0.05
CalcTotal	99.02	99.58	99.85	99.52	98.71	99.2	98.62	99.22	99.86	99.62	99.4	100.49	100.22
Mg#	20.947	23.984	15.963	16.72	0.000	13.421	11.924	14.167	39.806	18.332	39.034	16.859	10.622
Albite	28.616	20.211	24.533	54.223	25.528	54.69	20.423	19.718	26.961	22.93	38.072	44.765	43.675
Anorthite	71.142	79.678	75.272	45.125	74.367	44.601	79.382	80.083	72.725	76.831	61.602	54.916	56.005
Orthoclase	0.242	0.112	0.195	0.652	0.105	0.709	0.194	0.199	0.313	0.239	0.326	0.319	0.32

Table 5 (continued).

Sample no:	921B-3R-1, 71–79 cm						921C-2R-1, 70–78 cm					
Text. type:	3	3	3	3	3	3	2	2	2	3	3	3
	P	P	R	P	R	R	P	P	R	P	R	R
Na_2O	4.18	5.58	5.48	6.11	6.07	5.13	4	3.27	3.88	3.89	3.16	4.68
MgO	0.01	0.03	0.01	0.02	0.01	0.03	0.02	0.02	0.01	0.01	0.01	0
Al_2O_3	30.17	28.31	28.37	27.02	27.4	28.85	30.48	31.5	30.75	30.61	31.8	29.43
SiO_2	51.97	54.69	55.12	56.71	56.7	54.4	51.61	50.02	51.01	51.59	49.88	53.2
CaO	12.94	10.74	10.77	9.34	9.58	11.25	13.06	14.44	13.52	13.28	14.54	11.81
TiO_2	0.04	0.06	0.04	0.08	0.01	0.03	0.04	0.07	0.04	0.05	0.01	0.04
FeO	0.27	0.22	0.11	0.27	0.22	0.53	0.18	0.14	0.1	0.09	0.17	0.14
K_2O	0.04	0.07	0.09	0.11	0.06	0.1	0.06	0.05	0.04	0.01	0.01	0.01
CalcTotal	99.66	99.71	99.99	99.67	100.07	100.34	99.46	99.5	99.38	99.55	99.59	99.32
Mg#	7.392	18.841	11.295	10.159	9.011	8.667	16.532	18.755	11.295	12.671	13.32	0
Albite	36.814	48.261	47.677	53.897	53.215	44.937	35.527	29	34.089	34.605	28.201	41.734
Anorthite	62.972	51.34	51.779	45.482	46.444	54.498	64.117	70.731	65.674	65.336	71.758	58.225
Orthoclase	0.214	0.398	0.544	0.621	0.341	0.565	0.357	0.268	0.237	0.059	0.041	0.041

Table 6. Selected microprobe analyses of orthopyroxene (OPX), olivine (OL), amphibole (AM) and biotite (BI) in gabbroic rocks listed in Table 3.

	921E-2R-2, 54–60 cm					921E-7R-2, 70–75 cm								923A-2R-1, 13–16 cm					
Text. type:	1	4	4	1	4	0	0	4	4	4	4	0	4	3	3	3	3	3	3
Mineral	OL	OPX	OPX	AM	AM	OL	OL	OPX	OPX	OPX	OPX	AM	AM	OL	OL	OPX	OPX	AM	AM
	P	R	P	Int	R	P	P	R	P	P	P rim	Int		P	P	R	P	Incl	Int
Na_2O	0	0.02	0.02	2.85	2.93	0.03	0.01	0.02	0.04	0.03	0.02	2.53	2	0.01	0	0.03	0.04	3.02	2.9
Cr_2O_3	0	0	0	0.06	0	0	0.01	0.07	0	0	0.01	0.55	0.1	0	0	0.03	0.01	0.03	0.04
MgO	33.24	20.46	18.29	13.9	11.64	41	39.67	21.12	18.17	28.16	18.28	16.62	15.9	31.65	33.43	23.69	24.51	12.59	13.01
Al_2O_3	0	0.71	0.5	13.35	11.19	0	0	0.43	0.32	1.4	0.36	11.4	9.7	0	0	1.17	1.11	10.68	11
SiO_2	36.71	52.44	51.3	41.83	42.14	38.5	38.63	52.99	51.58	54.17	52	44.01	46.35	36.73	36.95	52.78	53.31	42.51	42.34
CaO	0.06	1.05	1.28	10.73	10.8	0.04	0.05	0.88	1.29	0.47	1.25	11.64	11.61	0.03	0.05	1.25	1.93	11.08	11.24
TiO_2	0.01	0.22	0.24	2.68	3.12	0.01	0.01	0.18	0.13	0.05	0.12	2.19	1.36	0.05	0.02	0.38	0.54	4.33	4.14
MnO	0.47	0.73	0.82	0.15	0.18	0.25	0.32	0.67	0.95	0.41	0.83	0.09	0.18	0.45	0.44	0.45	0.43	0.16	0.13
FeO	29.9	25.15	27.9	11.11	15.8	19.49	21.54	23.42	27.03	14.63	27.15	7.93	10.22	31.44	29.23	19.58	18.07	12.81	12.53
NiO	0.08	0	0.02	0.05	0.05	0.09	0.09	0.06	0	0.04	0.03			0.04	0.04	0.02	0.01	0	0.04
K_2O	0	0	0.01	0.28	0.22							0.13	0.19	0	0	0	0.01	0.18	0.18
CalcTotal	100.48	100.8	100.39	96.99	98.05	99.41	100.33	99.83	99.51	99.35	100.05	97.08	97.62	100.4	100.17	99.39	99.96	97.38	97.53
Mg#	66.465	59.186	53.881	69.034	56.779	78.951	76.653	61.65	54.509	77.436	54.555	78.899	73.498	64.216	67.094	68.327	70.737	63.668	64.923

Notes: Text. type = textural type; P = porphyroclast core; Prim = porphyroclast rim; R = recrystallized, Int = interstitial; Incl = inclusion in igneous pyroxene; Incl CPX = inclusion in clinopyroxene; Exs CPX = exsolution in clinopyroxene.

Table 6 (continued).

	923A-12R-2, 26–31 cm					921E-3R-1, 37–41 cm						921E-1R-1, 16–23 cm					
Text. type:	0	0	0	0	0	2	2	1	2	2	1	1	1	1	1	1	1
Mineral	OL	OL	OPX	OPX	AM	OPX	OPX	OPX	AM	AM	AM	OL	OPX	OPX	AM	AM	AM
	P	P	P	Int	Int	P	Incl CPX	P	Incl		Int	P	R	P	Int	Incl	
Na_2O	0.01	0.01	0	0.02	2.44	0.03	0.03	0.05	2.72	1.27	2.33	0	0.02	0.03	2.17	2.76	1.48
Cr_2O_3	0	0.01	0	0.03	0.11	0.02	0.04	0	0.03	0.01	0	0	0.03	0.03	0.05	0.11	0.01
MgO	39.1	36.11	26.61	26.95	15.4	19.23	19	17.62	10.88	9.67	12.07	31.06	24.39	24.77	14.78	13.37	13.6
Al_2O_3	0	0	1.03	1.03	11.51	0.73	1.13	0.58	10.81	6.8	10.16	0	1.15	1.34	11.31	11.38	8.2
SiO_2	37.98	37.17	54.05	53.84	43.57	52.29	51.86	51.87	42.62	46.79	43.74	36.13	53.59	53.31	44.13	43.02	47.47
CaO	0.04	0.05	0.96	1.14	11.82	1.4	1.15	2.18	10.51	10.89	10.39	0.01	1.25	1.94	11.06	10.85	11.34
TiO_2	0	0.03	0.36	0.43	2.8	0.26	0.23	0.28	3.65	1.03	2.86	0	0.37	0.5	2.43	4.1	0.76
MnO	0.31	0.32	0.38	0.37	0.07	0.75	0.72	0.78	0.24	0.26	0.23	0.46	0.45	0.38	0.16	0.14	0.17
FeO	22.61	25.92	16.82	15.79	8.55	26.12	26.51	26.68	15.96	20.63	15.23	31.82	18.78	16.82	10.06	11.06	13.15
NiO	0.05	0.09	0	0.02	0.03	0	0	0.02	0	0.02	0	0.06	0	0.02	0.05	0	0
K_2O	0	0.01	0	0.01	0.18	0	0	0.02	0.19	0.34	0.18	0	0	0	0.28	0.12	0.13
CalcTotal	100.11	99.73	100.21	99.65	96.47	100.84	100.67	100.1	97.61	97.72	97.18	99.55	100.02	99.16	96.5	96.91	96.3
Mg#	75.503	71.289	73.829	75.263	76.255	56.756	56.096	54.067	54.858	45.533	58.549	63.504	69.84	72.421	72.367	68.313	64.834

Table 6 (continued).

	921E-2R-2, 78–81 cm				921E-3R-1, 25–30 cm				923A-13R-1, 124–128 cm							
Text. type:	1	1	1	1	1	1	1	0	2	2	2	4	4	2	4	2
Mineral	OL	AM	AM	AM	OL	AM	AM	AM	OL	OL	OPX	OPX	OPX	AM	AM	AM
	P	Int	R		P		Incl	Int	P	R	Int	P	R		R	Int
Na_2O	0.00	2.44	2.45	1.75	0.01	0.8	2.68	1	0	0.02	0.02	0.01	0.02	0.33	2.71	2.98
Cr_2O_3	0.00	0.03	0.05	0	0.00	0.04	0.09	0	0.02	0	0.06	0.04	0.01	0.02	0.73	0.48
MgO	32.52	12.06	15.15	15.38	27.21	12.29	13.09	12.54	34.33	34.55	27.18	23.88	23.99	13.67	13.73	15.09
Al_2O_3	0.00	11.78	11.88	10.13	0.00	4.35	11.35	4.23	0	0.01	0.97	1.05	0.96	2.96	11.36	11.86
SiO_2	37.11	42.63	43.99	47.78	35.96	50.12	42.47	49.41	38.48	38.37	55.89	54.3	54.12	51.81	43.44	43.86
CaO	0.03	11.28	11.45	11.96	0.04	11.22	11.23	10.01	0.06	0.01	1.01	1.17	1.11	14.89	11.34	11.55
TiO_2	0.01	3.4	2.12	0.51	0.00	0.71	4.62	0.96	0	0.03	0.22	0.35	0.25	0.31	3.49	3.52
MnO	0.50	0.16	0.11	0.12	0.58	0.29	0.19	0.35	0.41	0.38	0.37	0.48	0.43	0.41	0.16	0.11
FeO	30.63	14.12	10.48	10.39	37.65	18.31	12	18.75	26.87	27.05	15.2	19.04	19.7	12.33	10.74	8.24
NiO	0.09	0.05	0.03	0	0.04	0.01	0	0.01	0.08	0.06	0	0	0.02	0.01	0.03	0.02
K_2O	0.00	0.22	0.17	0.13	0.01	0.17	0.09	0.18	0	0	0	0	0	0.05	0.2	0.23
CalcTotal	100.90	98.18	97.89	98.16	101.51	98.31	97.8	97.44	100.25	100.47	100.93	100.33	100.62	96.79	97.93	97.92
Mg#	65.430	60.353	72.035	72.512	56.296	54.469	66.041	54.385	69.49	69.48	76.119	69.094	68.462	66.402	69.514	76.548

Table 6 (continued).

	923A-13R-1, 136–142 cm								923A-2R-2, 30–33 cm											
Text. type:	4	3	3	3	4	3	3	4	4	1	2	4	4	3	1	4	4	1	4	4
Mineral	OL	OPX	OPX	OPX	OPX	AM	AM	AM	OL	OL	OPX	OPX	OPX	OPX	OPX	AM	AM	AM	BI	BI
	R	P	R	R	R	Incl	R	R	R	P	R	P	R	P	P	R		Int	P	P
Na_2O	0.000	0.04	0.02	0.02	0.02	2.91	2.97	2.88	0	0	0.04	0.02	0.02	0.01	0.03	2.65	1.95	2.64	0.26	0.59
Cr_2O_3	0.01	0.01	0.000	0.12	0.03	0.07	0.4	0.34	0	0	0	0.01	0	0.04	0	0.02	0	0.02	0.04	0.03
MgO	33.67	24.54	23.6	25.66	26.27	12.91	13.91	14.25	30.66	30.3	23.33	24.11	23.83	22.85	23.2	13.58	12.69	13.09	16.43	16.5
Al_2O_3	0.000	1.31	0.95	1.43	1.13	11.26	11.2	11.82	0	0	0.91	1.1	0.79	1.01	1.22	11.57	9.05	11.53	13.15	13.53
SiO_2	37.19	53.88	53.53	54.15	54.5	42.25	42.85	42.98	35.66	36.29	52.71	52.77	54.09	53.03	53.87	42.18	46.1	43.59	39.09	39.87
CaO	0.07	1.94	1.23	1.11	1.08	11.32	11.34	11.33	0.01	0.06	1.63	1.28	0.84	1.62	1.8	11.12	11.84	11.62	0.03	0.07
TiO_2	0.04	0.41	0.28	0.36	0.26	4.44	4.27	3.88	0.04	0.01	0.33	0.27	0.17	0.34	0.5	3.56	0.81	3.28	1.81	2.23
MnO	0.44	0.41	0.48	0.41	0.45	0.18	0.16	0.15	0.52	0.46	0.52	0.52	0.57	0.55	0.53	0.14	0.22	0.21	0.09	0.1
FeO	28.81	17.86	19.74	17.31	16.72	12.73	10.47	10.29	33.73	33.49	20.87	20.21	20.31	21.07	19.16	12.76	14.85	12.48	16.34	14.77
NiO	0.04	0.01	0.02	0.02	0.04	0.03	0.05	0.05	0.08	0.1	0.04	0.05	0.06	0	0	0	0	0	0.01	0.05
K_2O	0.000	0.000	0.000	0.000	0.000	0.34	0.12	0.17	0	0	0	0.01	0.01	0	0	0.25	0.32	0.23	7.06	7.98
CalcTotal	100.25	100.41	99.85	100.59	100.51	98.44	97.74	98.13	100.69	100.71	100.38	100.35	100.69	100.53	100.32	97.83	97.85	98.68	94.3	95.73
Mg#	67.567	71.014	68.067	72.548	73.685	64.392	70.311	71.168	61.838	61.721	66.588	68.02	67.648	65.906	68.332	65.478	60.374	65.149	64.196	66.563

Table 6 (continued).

	921E-7R-2, 94–100 cm	921E-3R-1, 3–9 cm						923A-16R-4, 85–89 cm			923A-11R-1, 95–101 cm				923A-3R-2, 51–57 cm		
Text. type:	0	3	3	3	3	3	3	2	2	0	2	4	4	2	4	0	2
Mineral	AM	OPX	OPX	OPX	OPX	AM	AM	OL	AM	AM	OL	OPX	OPX	AM	OPX	AM	AM
	Int	P	R	P	R	Incl	R	P	Int	Int	P	P	R	Incl	P	Int	Incl
Na_2O	0.94	0.02	0.01	0.03	0.01	2.71	2.59	0.000	2.63	1.12	0.02	0.03	0	2.88	0.04	2.39	2.59
Cr_2O_3	0	0.01	0.01	0	0.02	0.11	0.16	0.000	0.12	0.000	0	0.03	0.04	0.09	0.01	0.02	0
MgO	14.09	22.54	22.69	19.76	18.86	11.37	12.3	33.1	13.8	13.93	33.8	24.68	24.68	13.6	22.24	12.79	12.62
Al_2O_3	3.86	1.1	0.66	0.95	0.59	10.65	10.47	0.000	10.71	3.65	0.01	1.38	1.21	11.37	0.98	10.01	10.18
SiO_2	50.41	52.38	52.79	51.75	51.45	42.44	43.16	37.18	43.19	49.85	37.65	53.74	53.53	42.35	53.04	43.21	43.24
CaO	9.97	1.14	1.04	1.25	1.38	10.66	10.92	0.03	11.23	10.36	0.02	1.83	1.26	11.45	1.57	10.88	10.84
TiO_2	0.31	0.42	0.24	0.36	0.22	3.68	3.01	0.03	3.27	1.07	0.02	0.55	0.44	3.73	0.43	3.07	3.43
MnO	0.44	0.43	0.55	0.64	0.69	0.2	0.19	0.43	0.13	0.38	0.45	0.41	0.42	0.17	0.55	0.21	0.17
FeO	16.22	21.52	21.17	24.47	25.66	14.66	14.14	29.48	11.25	15.38	28.26	16.89	17.72	11.34	20.84	13.72	13.59
NiO	0.01	0.01	0	0.01	0.03	0	0.04	0.06	0.04	0.05	0.07	0	0.02	0.02	0.03	0.01	0.03
K_2O	0.13	0	0	0	0	0.13	0.21	0.000	0.26	0.19	0	0	0.03	0.11	0	0.23	0.19
CalcTotal	96.4	99.56	99.17	99.22	98.92	96.61	97.18	100.31	96.65	95.96	100.28	99.53	99.34	97.1	99.7	96.55	96.88
Mg#	60.766	65.115	65.645	59.006	56.716	58.021	60.794	66.678	68.621	61.746	68.067	72.254	71.291	68.133	65.541	62.431	62.332

Table 6 (continued).

	923A-8R-1, 31–46 cm				923A-15R-2, 0–6 cm		923A-16R-4, 6-12 cm		922A-2R-2, 106–111 cm							
Text. type:	0	0	0	0	1	1	0	0	3	3	3	3	3	4	4	4
Mineral	OL	OL	AM	AM	OL	AM	AM	AM	OL	OL	OL	OL	OL	OPX	OPX	AM
	P	P	Int	Int	P	Int	Int	Int	R	R	P	P	R	P	R	Int
Na_2O	0	0	2.27	2.21	0	2.38	2.68	0.88	0.03	0.02	0.04	0.01	0.000	0.04	0.06	2.17
Cr_2O_3	0	0.02	0.12	0.16	0	0.09	0.09	0.01	0	0	0	0	0.01	0.03	0.01	0.13
MgO	39.25	38.68	14.83	15.66	33.85	12.48	11.6	12.34	42.75	40.58	40.18	41.83	39.33	20.44	22.47	13.94
Al_2O_3	0	0	10.64	11.53	0.01	11.83	9.74	3.93	0	0.01	0	0	0.000	0.75	1.01	10.42
SiO_2	37.4	39.25	43.59	44.67	37.69	42.24	42.48	49.21	38.86	38.62	38.31	38.95	38.54	51.99	52.77	43.76
CaO	0.04	0.05	11.8	11.69	0.01	11.55	10.76	11.38	0.02	0.02	0.04	0.01	0.01	1.58	1.25	11.5
TiO_2	0.02	0	3.6	3.19	0.01	3.13	3.46	0.6	0	0.01	0.03	0.02	0.01	0.31	0.31	3.1
MnO	0.38	0.35	0.13	0.14	0.42	0.18	0.26	0.39	0.26	0.38	0.37	0.31	0.35	0.77	0.67	0.15
FeO	23.24	21.88	9.74	8.04	28.36	12.05	14.98	18.01	17.7	20.39	20.6	18.66	21.78	23.46	20.63	11.33
NiO	0.11	0.14	0.04	0	0.03	0.04	0.03	0.02	0.17	0.15	0.13	0.15	0.13	0.01	0.05	0.06
K_2O	0	0	0.26	0.22	0	0.38	0.2	0.21					0.000			0.39
CalcTotal	100.44	100.38	97.01	97.51	100.39	96.36	96.29	96.98	99.79	100.18	99.7	99.95	100.18	99.37	99.24	96.94
Mg#	75.066	75.911	73.084	77.644	68.03	64.862	57.983	54.977	81.153	78.008	77.661	79.979	76.299	60.839	66.006	68.692

Table 6 (continued).

	922A-2R-2, 123–128 cm							922A-2R-2, 56–62 cm				922B-4R-1, 59–63 cm					
Text. type:	0	0	4	4	4	3	0	0	4	0	4	4	4	1	4	4	4
Mineral	OL	OL	OPX	OPX	OPX	AM	AM	OL	OPX	OPX	AM	AM	AM	AM	AM	AM	AM
	P	P	R	P	P	R	Int	P	P	Exs CPX	P	Incl Plag		R	Int		Int
Na_2O	0	0	0.03	0.02	0.04	2.91	2.6	0	0.01	0.05	2.35	2.51	1.34	2.34	2.38	0.47	1.42
Cr_2O_3	0	0.01	0	0.02	0	0.13	0.22	0	0.01	0.2	0.05	0.01	0.01	0.02	0.05	0	0.02
MgO	45.16	41.84	24.07	24.34	22.73	15.03	16.75	45.77	29.95	29.68	16.22	14.34	14.04	14.59	14.85	15.45	12.77
Al_2O_3	0	0.01	0.62	0.71	0.88	11.59	11.07	0	0.65	1.39	10.56	12.39	7.05	11.57	10.77	2.5	7.04
SiO_2	39.66	38.94	53.27	53.31	52.78	42.2	43.61	38.97	55.15	54.58	43.89	42.85	48.29	44.34	45.31	54.43	47.94
CaO	0.06	0.08	1.22	1.3	1.28	11.77	12.08	0.05	0.95	3.23	11.52	11.76	11.93	11.42	11.61	12.71	10.82
TiO_2	0.04	0.02	0.21	0.36	0.28	3.99	4.54	0.01	0.32	0.5	4.14	3.5	0.98	2.78	3.3	0.24	1.61
MnO	0.23	0.31	0.47	0.5	0.61	0.08	0.07	0.24	0.3	0.3	0.12	0.14	0.2	0.2	0.14	0.27	0.24
FeO	14.78	18.91	19.78	19.47	20.87	7.87	5.59	14.58	12.56	9.89	7.13	10.18	14	10.49	9.16	12.36	15.82
NiO	0.18	0.17	0.04	0.04	0.06		0.08	0.17	0.02	0.05	0.05	0.06	0.08	0.06	0.03	0.02	0.05
K_2O	0.01	0	0	0		0.28	0.31	0	0	0.01	0.45	0.37	0.31	0.27	0.34	0.04	0.22
CalcTotal	100.13	100.29	99.72	100.08	99.54	95.87	96.92	99.79	99.92	99.89	96.47	98.1	98.25	98.08	97.91	98.5	97.96
Mg#	84.491	79.771	68.448	69.029	66.003	77.292	84.239	84.837	80.954	84.246	80.223	71.513	64.126	71.259	74.294	69.028	58.99

Table 6 (continued).

	922A-2R-6, 18–25 cm												922A-3R-1, 63–66 cm								
Text. type:	1	1	1	3	3	1	3	0	3	3	1	1	4	1	1	4	4	4	4	4	1
Mineral	OL	OL	OL	OPX	OPX	OPX	AM	AM	AM	AM	AM	AM	OL	OL	OL	OPX	OPX	OPX	AM	AM	AM
	P	R	P	P	P	R	R	Int		Int	Int	Int	P	P	P	P	P	R	R	R	Int
Na_2O	0.000	0.000	0.01	0.03	0.03	0.01	2.57	1.55	2.45	2.4	2.51	2.71	0.01	0	0	0.01	0.01	0.02	2.68	2.77	2.58
Cr_2O_3	0.01	0.000	0.000	0.01	0.000	0.07	0.05	0.01	0.27	0.04	0.31	0.97	0	0	0	0	0.01	0.01	0.16	0	0.37
MgO	37.76	34.5	40.93	25.000	21.05	30.96	15.34	11.95	12.29	15.24	13.94	16.14	42.58	44.91	33.11	23.11	22.85	24.7	16.54	10.52	16.81
Al_2O_3	0.000	0.000	0.000	0.88	0.87	1.33	12.92	6.46	10.76	9.81	10.93	11.29	0	0	0	0.77	0.83	0.99	12.4	13.39	11.77
SiO_2	37.73	37.06	38.83	53.62	52.25	55.32	43.27	47.28	43.21	44.66	43.08	43.07	38.72	39.2	35.99	51.41	52.35	52.28	43.38	41.23	42.94
CaO	0.02	0.02	0.05	2.02	1.88	0.78	10.56	10.76	11.000	11.11	11.73	11.86	0.02	0.06	0.05	1.29	1.12	1.33	11.12	11.45	12.09
TiO_2	0.000	0.02	0.01	0.39	0.34	0.29	2.72	1.52	2.9	3.19	3.35	3.2	0.03	0	0.02	0.32	0.34	0.35	3.55	0.2	4.24
MnO	0.38	0.42	0.29	0.52	0.58	0.28	0.2	0.32	0.26	0.23	0.2	0.08	0.28	0.25	0.56	0.63	0.7	0.57	0.11	0.29	0.08
FeO	23.66	27.73	19.3	17.12	22.6	10.78	9.39	17.3	14.5	9.87	10.75	6.58	18.8	15.82	29.94	20.8	22	18.86	6.79	16.08	5.48
NiO	0.14	0.12	0.17	0.04	0.000	0.04	0.05	0.000	0.02	0.1	0.02	0.02	0.15	0.22	0.07	0.01	0.03	0	0.05	0.04	0.04
K_2O	0.000	0.000	0.000	0.000	0.000	0.000	0.24	0.28	0.24	0.2	0.25	0.17	0	0	0	0	0	0	0.24	0.12	0.19
CalcTotal	99.71	99.86	99.58	99.63	99.62	99.86	97.3	97.44	97.9	96.85	97.07	96.09	100.6	100.46	99.74	98.36	100.23	99.12	97.03	96.09	96.59
Mg#	73.987	68.925	79.082	72.25	62.408	83.662	74.452	55.174	60.172	73.35	69.792	81.381	80.147	83.499	66.347	66.452	64.927	70.006	81.294	53.846	84.549

Table 6 (continued).

	921B-3R-1, 33–36 cm		921B-3R-1, 94–99 cm				922B-1W-1, 109–115 cm														
Text. type:	3	3	2	3	3	2	1	1	1	4	4	4	3	3	3	4	1	3	3	4	1
Mineral	OPX	AM	OL	OPX	OPX	AM	OL	OL	OL	OL	OL	OL	OPX	OPX	OPX	OPX	AM	AM	AM	AM	AM
	P	Int	R	P	P	Int	P	P	P	P	R	R	P	P	R	R	R	R	R	R	Int
Na_2O	0.04	2.79	0.000	0.05	0.03	2.67	0.01	0	0.01	0.01	0	0.01	0.05	0.01	0.02	0.02	2.85	2.84	0.16	2.72	2.66
Cr_2O_3	0.01	0.01	0.000	0.03	0.02	0.09	0.01	0	0	0.01	0	0	0.01	0.03	0.000	0.04	0.56	0.02	0.000	0.12	0.52
MgO	20.87	11.9	31.61	23.6	19.22	13.88	33.68	41.04	43.5	45.37	45.05	38.93	20.32	24.85	25.53	28.55	15.49	14.09	20.35	15.61	15.69
Al_2O_3	1.03	11.1	0.000	1.16	0.56	10.29	0.000	0	0	0	0	0	0.8	0.89	0.94	1.2	11.92	11.38	1.35	12.06	11.44
SiO_2	52.46	42.78	36.44	53.43	51.85	44.39	36.46	38.52	38.47	39.07	39.42	37.54	52.06	53.41	53.55	54.12	42.54	42.49	52.35	42.78	42.77
CaO	1.57	10.72	0.04	2.51	1.47	11.05	0.06	0.04	0.03	0.04	0.01	0.02	1.79	1.09	1.17	0.97	11.48	11.35	10.35	11.35	11.88
TiO_2	0.35	4.64	0.01	0.44	0.31	3.86	0.000	0	0.02	0.02	0	0.02	0.36	0.26	0.28	0.31	3.9	3.74	0.37	3.63	4.17
MnO	0.61	0.19	0.51	0.43	0.65	0.14	0.5	0.35	0.3	0.25	0.25	0.37	0.72	0.47	0.48	0.42	0.12	0.16	0.43	0.14	0.1
FeO	23.46	14.5	32.02	18.4	25.68	11.66	28.2	20.85	17.72	15.53	15.81	23.5	23.14	17.45	16.63	14.28	7.1	9.53	12.46	8.4	6.98
NiO	0.04	0.01	0.08	0.000	0.02	0.03	0.1	0.2	0.16	0.16	0.19	0.19	0.01	0.05	0.05	0.04	0.04	0.04	0.08	0.04	0.09
K_2O	0.01	0.18	0.000	0.02	0.000	0.15	0.000	0	0	0	0	0.01	0.01	0.000	0.000	0.02	0.29	0.27	0.000	0.35	0.39
CalcTotal	100.44	98.8	100.72	100.06	99.81	98.2	99.02	101.02	100.21	100.45	100.74	100.59	99.27	98.51	98.64	99.97	96.29	95.9	97.88	97.21	96.68
Mg#	61.329	59.399	63.759	69.573	57.158	67.967	68.043	77.819	81.401	83.888	83.551	74.705	61.02	71.742	73.237	78.081	79.544	72.495	74.433	76.804	80.032

Table 6 (continued).

	921B-3R-1, 134–137 cm		921B-3R-1, 71–79 cm								921C-2R-1, 70–78 cm					
Text. type:	0	0	3	3	3	3	3	3	3	3	3	3	3	3	3	2
Mineral	OL	AM	OL	OL	OL	OPX	OPX	OPX	OPX	AM	OL	OL	OPX	AM	AM	AM
	P	Int	P	R	R	Incl CPX	P	R	R	Incl	R	P	R	Int	Int	Int
Na_2O	0	2.5	0.01	0.01	0.02	0.01	0.06	0.01	0.04	2.51	0.01	0.01	0.03	2.86	2.6	
Cr_2O_3	0	0.11	0	0	0.02	0.08	0.02	0	0.01	0	0.02	0.01	0.11	0.91	0.47	
MgO	34.68	14.14	33.64	30.44	26.87	24.75	19.27	18.89	21.87	10.37	38.46	39.46	27.85	15.47	14.25	
Al_2O_3	0.01	10.7	0	0	0	1.66	0.92	0.76	0.78	9.31	0.02	0.01	1.13	11.86	11.31	
SiO_2	38.4	43.77	37.14	36.53	35.79	53.5	51.86	51.61	53.02	43.9	38.24	38.48	54.94	43.28	43.56	
CaO	0.04	11.32	0.04	0.03	0.06	0.82	1.5	1.45	1.19	10.7	0.01	0.04	0.87	11.6	11.56	
TiO_2	0.02	3.63	0.04	0.03	0.02	0.24	0.39	0.27	0.21	3.38	0	0	0.21	3.53	3.53	
MnO	0.44	0.14	0.38	0.49	0	0.35	0.7	0.7	0.57	0.29	0.3	0.26	0.3	0.12	0.1	
FeO	26.31	11.3	27.34	31.99	36.37	17.77	24.96	25.56	21.75	17	21.93	21	13.7	7.43	9.01	
NiO	0.03	0.02	0.08	0.05	0.07	0.05	0	0	0	0.03	0.12	0.08	0.04	0.04	0.07	
K_2O	0.02	0.17	0.04	0	0	0	0	0.01	0	0.15	0	0	0	0.15	0.15	
CalcTotal	99.96	97.79	98.7	99.58	99.21	99.23	99.69	99.26	99.43	97.65	99.1	99.35	99.17	97.24	96.62	
Mg#	70.148	69.047	68.686	62.918	56.845	71.288	57.92	56.855	64.186	52.094	75.769	77.011	78.379	78.788	73.829	

blasts. The euhedral grains are iron-rich (Mg# between 0.54 and 0.58), the anhedral grains near olivine are iron-poor (Mg# between 0.76 and 0.79). Olivine from the undeformed olivine gabbro has similarly high Mg#. Dynamically recrystallized orthopyroxene has intermediate Mg# values (0.57–0.63; Table 3; Fig. 9C). We propose that the high-Mg# orthopyroxene was produced by a reaction between xenocrysts of magnesian olivine and the gabbronoritic parental melt. The low-Mg# orthopyroxene would have crystallized directly from this melt. Slightly higher Mg# in orthopyroxene neoblasts could then reflect recrystallization in the presence of interstitial residual melt with slightly higher magnesium contents than the gabbronoritic parental melt. These slightly higher magnesium contents could be caused by the fractionation of iron oxides, or by chemical exchanges between the melt and the surrounding olivine gabbro.

DISCUSSION AND CONCLUSIONS

Ductile shear zones cored at Sites 921–923 localize preferentially in gabbronoritic intervals (although there are undeformed gabbronoritic intervals in the core; Fig. 3). The least-evolved gabbroic lithologies (troctolites) are rarely deformed, and the most-evolved lithologies (leucocratic segregations) are not deformed. A close look at ductile shear zones and at their mineral chemistry suggests that in many cases they developed in gabbronoritic dikelets intruded into less-evolved lithologies: (1) there are xenocrysts from these less-evolved rocks in some shear zones (Fig. 5A); (2) we interpret the rims of orthopyroxene that surround olivine xenocrysts as products of a reaction between these olivine xenocrysts and the gabbronoritic parental melt; and (3) high Mg# in igneous pyroxenes in some shear zones are best explained by buffering of the gabbronoritic parental melt by the magnesium-rich host gabbro. In most cases, these sheared gabbronoritic intervals contain small euhedral igneous minerals (Figs. 5D, 5E) and therefore probably had fine igneous grain sizes.

Recrystallized phase assemblages are similar to igneous ones in most deformed samples. This indicates that ductile deformation occurred in high-temperature nearly anhydrous conditions similar to magmatic conditions. Compositional variations in igneous and recrystallized minerals in many shear zones also suggest that ductile deformation took place with some residual melt present: variations in An content of recrystallized plagioclase, variations in Mg# of recrystallized orthopyroxene, and the existence of undeformed leucocratic patches with sodium-rich plagioclase (Fig. 5B) are best explained by interactions between the deforming gabbro, and an interstitial melt of a more evolved sodium- and silica-rich composition. The presence of interstitial melt in shear zones during deformation would produce a strong rheological contrast between material in the shear zone and the surrounding rocks. It is therefore also consistent with observations that extensively deformed intervals in the core are commonly juxtaposed with undeformed or weakly deformed gabbros (Figs. 2A, 5A).

The range of gabbroic lithologies recovered at Sites 921–923 in the MARK area, their relative proportions in the core, the composition of igneous minerals, the preferred localization of ductile deformation in gabbronoritic lithologies, and the probable role of trapped fractionated melts in favoring this strain localization recall observations made at Site 735 in the Southwest Indian Ocean (Bloomer et al., 1991; Natland et al., 1991; Dick et al., 1991). Bloomer et al. (1991) proposed a schematic model for the crystallization of gabbroic rocks at this site. In Figure 12, we show a modified version of this model, adapted to fit our observations at Sites 921–923. This model shows an irregularly shaped magma body that crystallizes troctolitic cumulates on its margins and that is progressively cooled (Fig. 12A). As crystallization proceeds, the porosity that kept melt circulating through the cumulate pile is closed, and trapped melts begin to fractionate. In Figure 12B, the cumulate pile behaves as a solid transmitting tectonic stresses. Evolved residual melts are pressed out of the

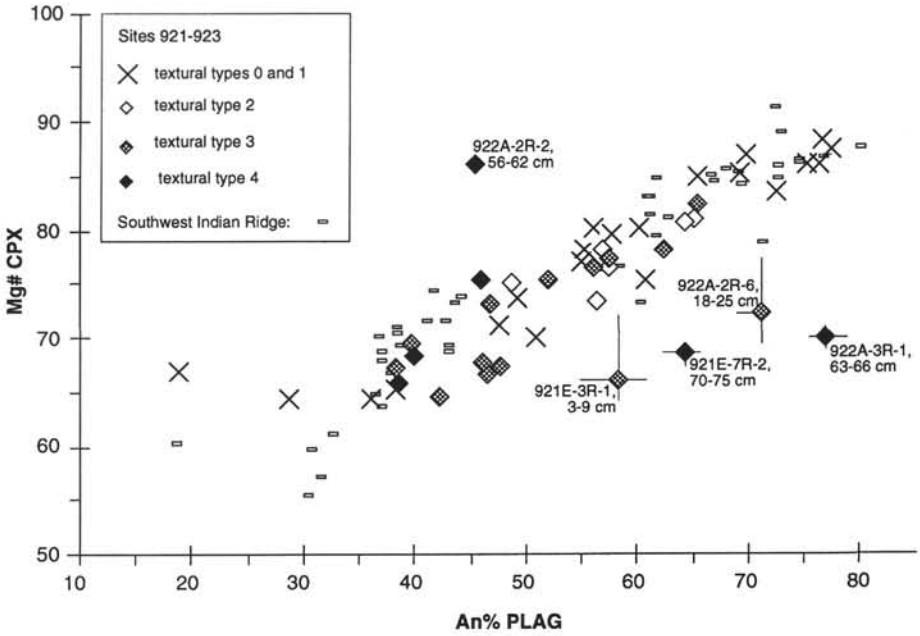

Figure 6. Average Mg# in clinopyroxene vs. average An content in plagioclase for the variably deformed gabbroic rocks listed in Table 3. Southwest Indian Ridge samples come from Hole 735B (Ozawa et al., 1991), and from other ridge and transform locations (Meyer et al., 1989). Ranges of compositional variations are shown for samples that do not plot on the tholeiitic differentiation trend. Ranges for other samples are listed in Table 3. CPX = clinopyroxene, PLAG = plagioclase.

cumulates and shear zones develop wherever these melts pond. It is possible that these melts pond wherever shear stress concentrations favor fracturing and veining. A complex interplay may therefore develop between melt migration paths and stress patterns in the cumulate pile. As pointed out by Bloomer et al. (1991), and by Natland et al. (1991) for the Site 735 case, gravity could also play a role in controlling the migration of residual melts, iron-rich evolved melts being substantially denser than the magnesium-rich olivine gabbro and troctolite matrix. In Figure 12C, most residual melts have crystallized, only the very last leucocratic segregates are still liquid. Ductile deformation in the small shear zones that we cored in the MARK area appears to have stopped at this stage.

The core from Sites 921 to 923 lacks the meter- to decameter-thick sheared intervals that were observed at Site 735 in the Southwest Indian Ocean (Dick et al., 1991; Cannat et al., 1991). Another difference that is striking concerns the involvement of high-temperature hydrothermal alteration products in the ductile deformation: sheared amphibolites are common at Site 735 (Stakes et al., 1991) but are virtually absent from the gabbroic core from the MARK area (Cannat, Karson, Miller, et al., 1995). The interpretation for Site 735 was that seawater-derived fluids had been introduced into the hot regions of the deforming axial lithosphere along large offset faults and thick shear zones that branched all the way up to the seafloor (Cannat et al., 1991; Mével and Cannat, 1991). Following this interpretation, the absence of such thick shear zones in the core recovered from Sites 921 to 923 could explain why amphibolite facies hydrothermal alteration is virtually lacking in this core (Cannat, Karson, Miller, et al., 1995). We should not conclude, however, that amphibolite facies alteration and sheared amphibolites that may have formed in and near thick ductile shear zones are absent in the MARK area gabbros. First, the core recovered from Sites 921 to 923 represents only about 30% of the material that was drilled at these sites (Table 1). It is therefore possible that thick shear zones were drilled through, but not recovered. Second, samples collected during the three submersible diving cruises devoted to the gabbroic outcrops in the vicinity of the drill sites do include amphibolitized gabbros and sheared amphibolites similar to the Site 735 samples (Karson and Dick, 1983; Marion, 1992; Gillis et al., 1993; I. Ghose et al., unpubl. data). It is therefore probable that thick shear zones similar to the ones at Site 735 have been active in the MARK area, but that we have not sampled them during Leg 153.

ACKNOWLEDGMENTS

We thank our two reviewers for their thorough and helpful work on the paper. We also thank the captain, the crew, and the drilling and technical staff of the *JOIDES Resolution.* Financial support for our work was provided by INSU-CNRS ("Géosciences marines" program).

REFERENCES

Auzende, J.-M., Cannat, M., Gente, P., Henriet, J.P., Juteau, T., Karson, J., Lagabrielle, Y., Mével, C., and Tivey, M., 1993. Affleurements des roches profondes de la croûte océanique et du manteau sur le mur Sud de la fracture Kane (Atlantique Central): observations par submersible. *C.R. Acad. Sci. Ser. 2,* 317:1641–1648.

Bloomer, S.H., Meyer, P.S., Dick, H.J.B., Ozawa, K., and Natland, J.H., 1991. Textural and mineralogic variations in gabbroic rocks from Hole 735B. *In* Von Herzen, R.P., Robinson, P.T., et al., *Proc. ODP, Sci. Results,* 118: College Station, TX (Ocean Drilling Program), 21–39.

Cannat, M., 1993. Emplacement of mantle rocks in the seafloor at mid-ocean ridges. *J. Geophys. Res.,* 98:4163–4172.

Cannat, M., and Casey, J.F., 1995. An ultramafic lift at the Mid-Atlantic Ridge: successive stages of magmatism in serpentinized peridotites from the 15°N region. *In* Vissers, R.L.M., and Nicolas, A. (Eds.), *Mantle and Lower Crust Exposed in Oceanic Ridges and Ophiolites:* Dordrecht (Kluwer), 5–34.

Cannat, M., Mével, C., and Stakes, D., 1991. Normal ductile shear zones at an oceanic spreading ridge: tectonic evolution of Site 735 gabbros (southwest Indian Ocean). *In* Von Herzen, R.P., Robinson, P.T., et al., *Proc. ODP, Sci. Results,* 118: College Station, TX (Ocean Drilling Program), 415–429.

Cannat, M., Karson, J.A., Miller, D.J., et al., 1995. *Proc. ODP, Init. Repts.,* 153: College Station, TX (Ocean Drilling Program).

Dick, H.J.B., Meyer, P.S., Bloomer, S., Kirby, S., Stakes, D., and Mawer, C., 1991. Lithostratigraphic evolution of an in-situ section of oceanic Layer 3. *In* Von Herzen, R.P., Robinson, P.T., et al., *Proc. ODP, Sci. Results,* 118: College Station, TX (Ocean Drilling Program), 439–538.

Dick, H.J.B., Thompson, G., and Bryan, W.B., 1981. Low angle faulting and steady state emplacement of plutonic rocks at ridge-transform intersections. *Eos,* 62:406.

Gente, P., Pockalny, R., Durand, C., Deplus, C., Maia, M., Ceuleneer, G., Mével, C., Cannat, M., and Laverne, C., 1995. Characteristics and evolution of the segmentation of the Mid-Atlantic Ridge between 20°N and 24°N during the last 10 million years. *Earth Planet. Sci. Lett.,* 129:55–71.

Helmstaedt, H., and Allen, J.M., 1977. Metagabbronorite from DSDP Hole 334: an example of high-temperature deformation and recrystallization near the Mid-Atlantic ridge. *Can. J. Earth Sci.,* 14:886–898.

Ito, E., and Anderson, A.T., Jr., 1983. Submarine metamorphism of gabbros from the Mid-Cayman Rise: petrographic and mineralogic constraints on hydrothermal processes at slow-spreading ridges. *Contrib. Mineral. Petrol.,* 82:371–388.

Karson, J.A., 1990. Seafloor spreading on the Mid-Atlantic Ridge: implications for the structure of ophiolites and oceanic lithosphere produced in slow-spreading environments. *In* Malpas, J., Moores, E.M., Panayiotou, A., and Xenophontos, C. (Eds.), *Ophiolites: Oceanic Crustal Analogues:* Proc. Symp. "Troodos 1987": Nicosia, Cyprus (Minist. Agric. Nat. Resour.), 547–555.

Karson, J.A., Thompson, G., Humphris, S.E., Edmond, J.M., Bryan, W.B., Brown, J.R., Winters, A.T., Pockalny, R.A., Casey, J.F., Campbell, A.C., Klinkhammer, G., Palmer, M.R., Kinzler, R.J., and Sulanowska, M.M., 1987. Along-axis variations in seafloor spreading in the MARK area. *Nature,* 328:681–685.

Mével, C., and Cannat, M., 1991. Lithospheric stretching and hydrothermal processes in oceanic gabbros from slow-spreading ridges. *In* Peters, T., Nicolas, A., and Coleman, R.J. (Eds.), *Ophiolite Genesis and Evolution of the Oceanic Lithosphere.* Petrol. Struct. Geol., 5:293–312.

Mével, C., Cannat, M., Gente, P., Marion, E., Auzende, J.-M., and Karson, J.A., 1991. Emplacement of deep crustal and mantle rocks on the west median valley wall of the MARK area (MAR 23°N). *Tectonophysics,* 190:31–53.

Meyer, P.S., Dick, H.J.B., and Thompson, G., 1989. Cumulate gabbros from the Southwest Indian Ridge, 54°S–7°16′E: implications for magmatic processes at a slow spreading ridge. *Contrib. Mineral. Petrol.,* 103:44–63.

Natland, J.H., Meyer, P.S., Dick, H.J.B., and Bloomer, S.H., 1991. Magmatic oxides and sulfides in gabbroic rocks from Hole 735B and the later development of the liquid line of descent. *In* Von Herzen, R.P., Robinson, P.T., et al., *Proc. ODP, Sci. Results,* 118: College Station, TX (Ocean Drilling Program), 75–111.

Ozawa, K., Meyer, P.S., and Bloomer, S.H., 1991. Mineralogy and textures of iron-titanium oxide gabbros and associated olivine gabbros from Hole 735B. *In* Von Herzen, R.P., Robinson, P.T., et al., *Proc. ODP, Sci. Results,* 118: College Station, TX (Ocean Drilling Program), 41–73.

Shipboard Scientific Party, 1989. Site 735. *In* Robinson, P.T., Von Herzen, R., et al., *Proc. ODP, Init. Repts.,* 118: College Station, TX (Ocean Drilling Program), 89–222.

Stakes, D., Mével, C., Cannat, M., and Chaput, T., 1991. Metamorphic stratigraphy of Hole 735B. *In* Von Herzen, R.P., Robinson, P.T., et al., *Proc. ODP, Sci. Results,* 118: College Station, TX (Ocean Drilling Program), 153–180.

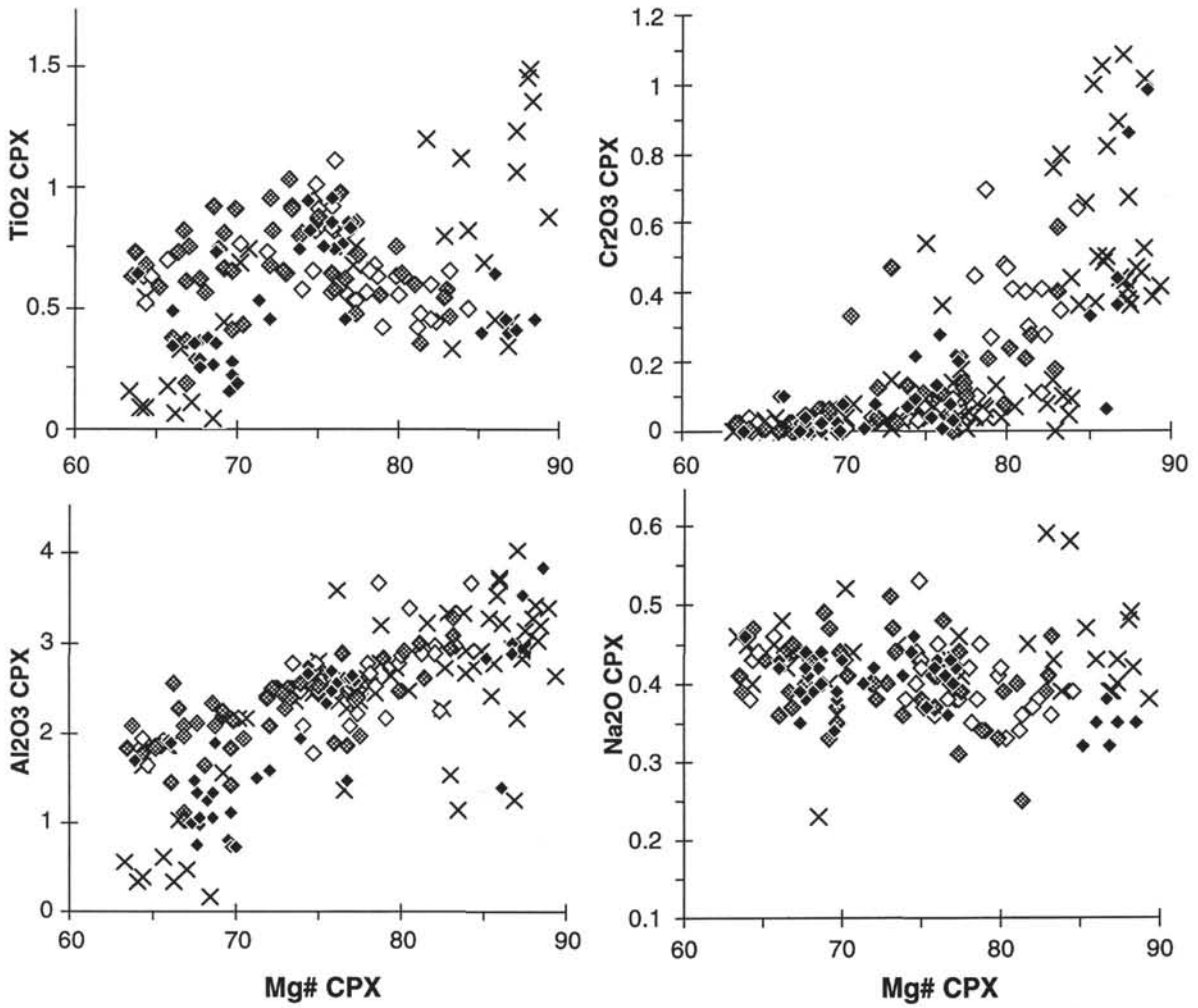

Figure. 7. Compositional variations in clinopyroxene from variably deformed gabbroic rocks cored at Sites 921, 922, and 923. Symbols and abbreviations are the same as in Figure 6.

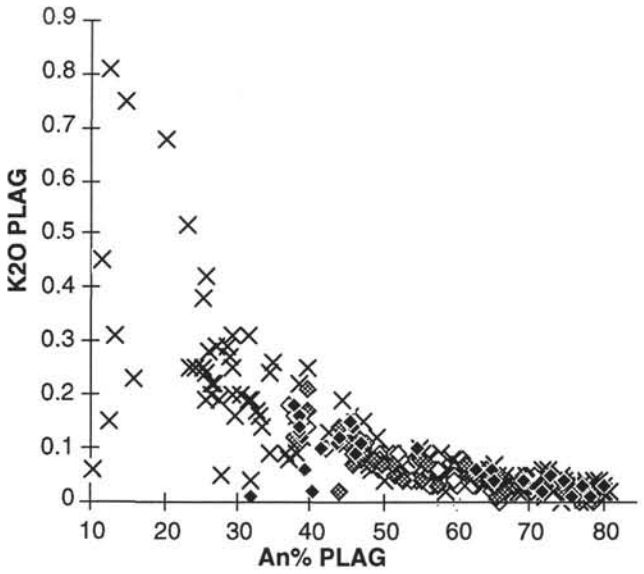

Figure. 8. K_2O% vs. An% in plagioclase from variably deformed gabbroic rocks cored at Sites 921, 922, and 923. Symbols and abbreviations are the same as in Figure 6.

Date of initial receipt: 7 August 1995
Date of acceptance: 26 January 1996
Ms 153SR-006

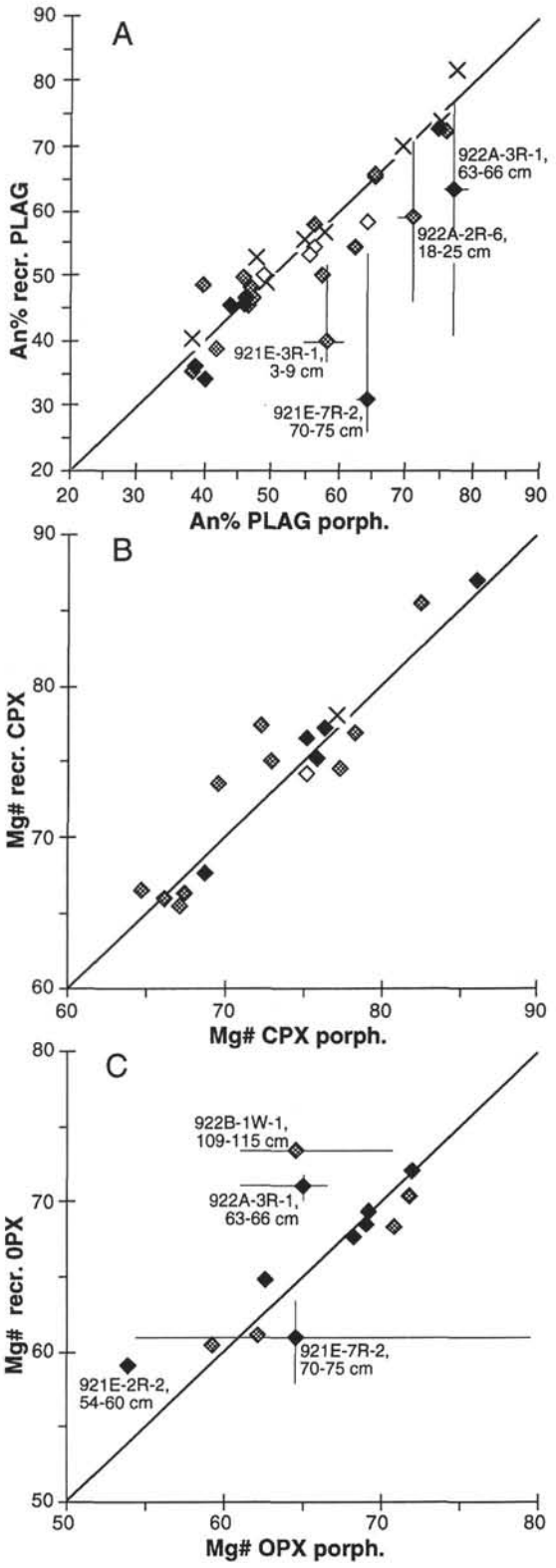

Figure 9. Average An% and Mg# of igneous and dynamically recrystallized **(A)** plagioclase, **(B)** clinopyroxene, and **(C)** orthopyroxene in deformed gabbroic rocks cored at Sites 921, 922, and 923. Oblique lines correspond to identical compositions for igneous and recrystallized grains. Ranges of variations are shown for selected samples in **A** and **C**. Other ranges of variation are listed in Table 3. Symbols and abbreviations are the same as in Figure 6; OPX = orthopyroxene, recr. = recrystallized, porph. = porphyroclast.

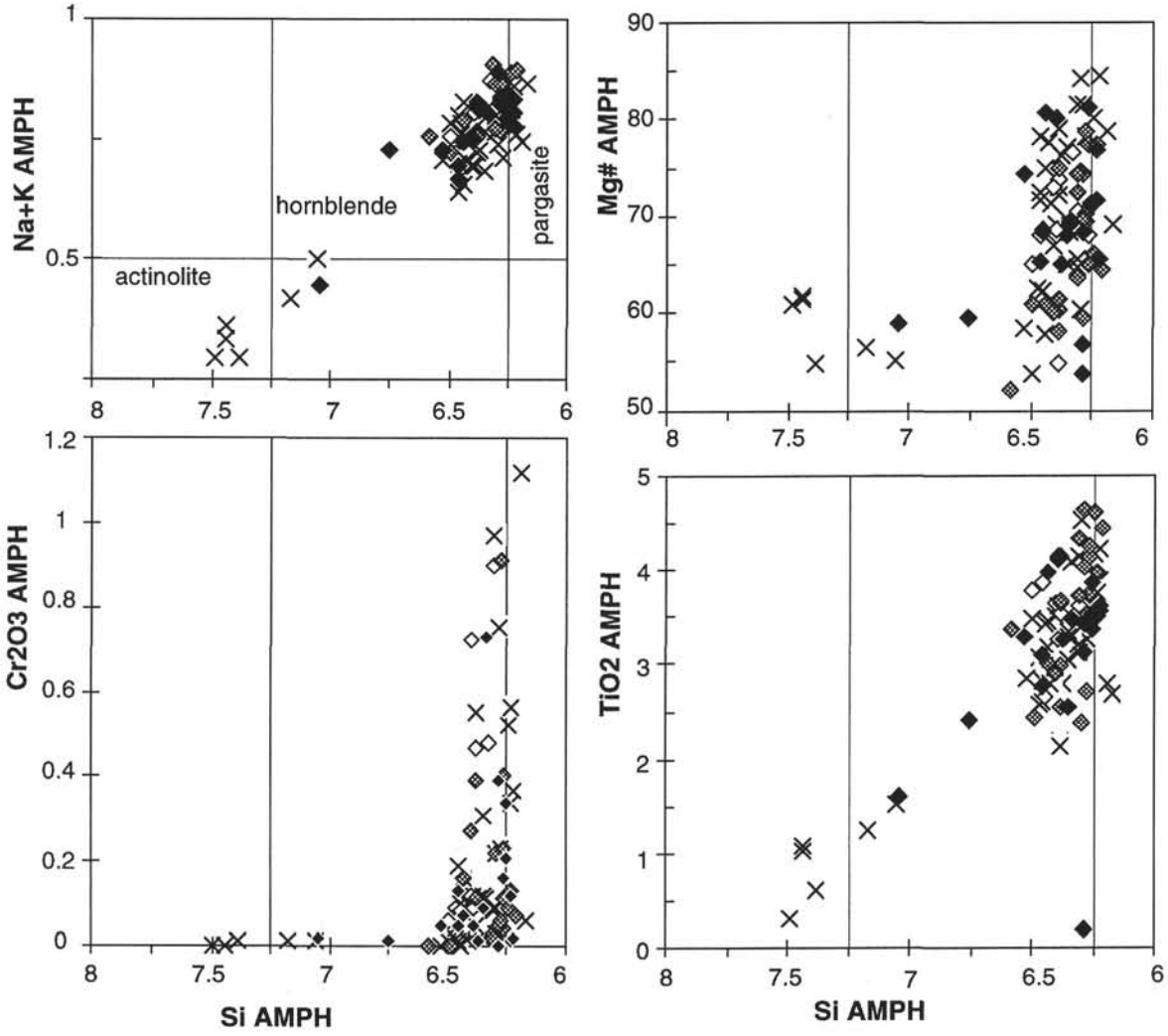

Figure 10. Compositional variations in brown to greenish brown amphibole from variably deformed gabbroic rocks cored at Sites 921, 922, and 923. Symbols are the same as in Figure 6; AMPH = amphibole.

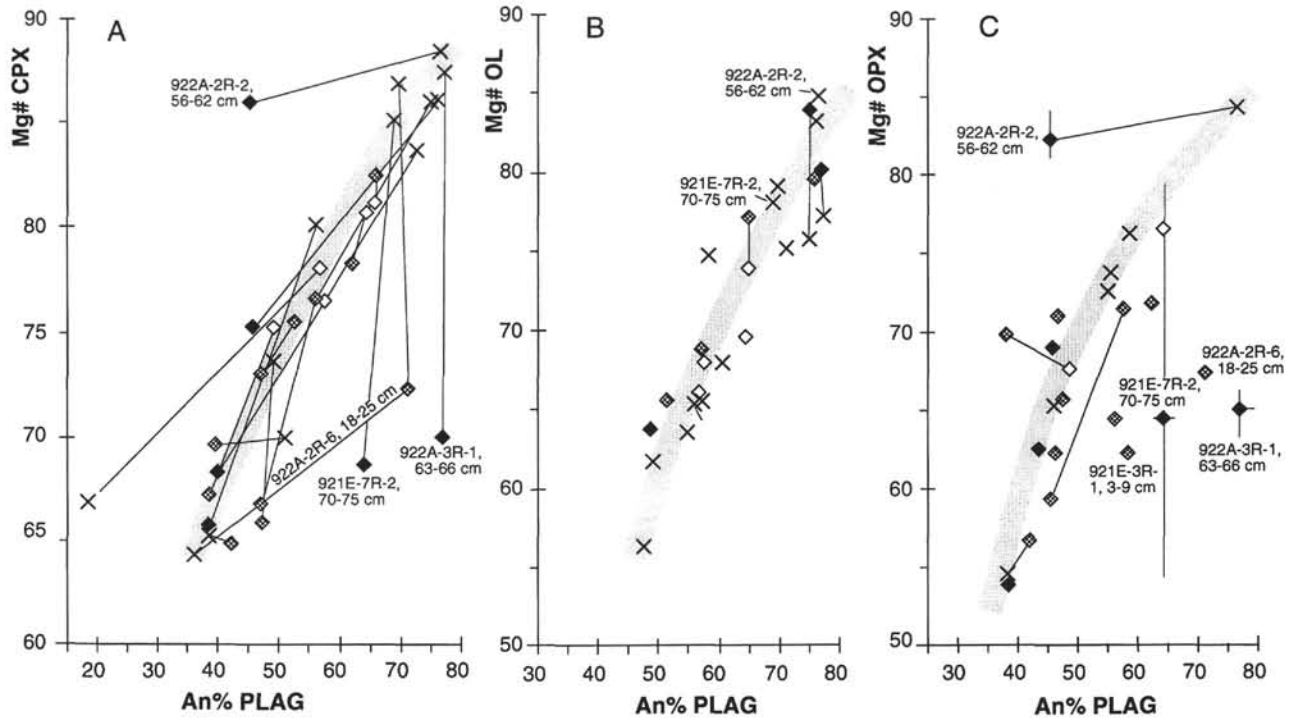

Figure 11. Compositional variations in **(A)** plagioclase and clinopyroxene, **(B)** plagioclase and olivine, and **(C)** plagioclase and orthopyroxene in deformed samples from Sites 921, 922, and 923 and in the less deformed gabbroic rocks that surround them. Mg# and anorthite contents plotted in this figure are average values. Ranges of variations are shown for selected samples in **C**. Ranges of variations for other samples are listed in Table 3. Lines connect variably deformed lithologies from the same piece of core. The thick gray lines show inferred differentiation trends, drawn based on the composition of the least deformed samples. Symbols and abbreviations are the same as in Figures 6 and 9.

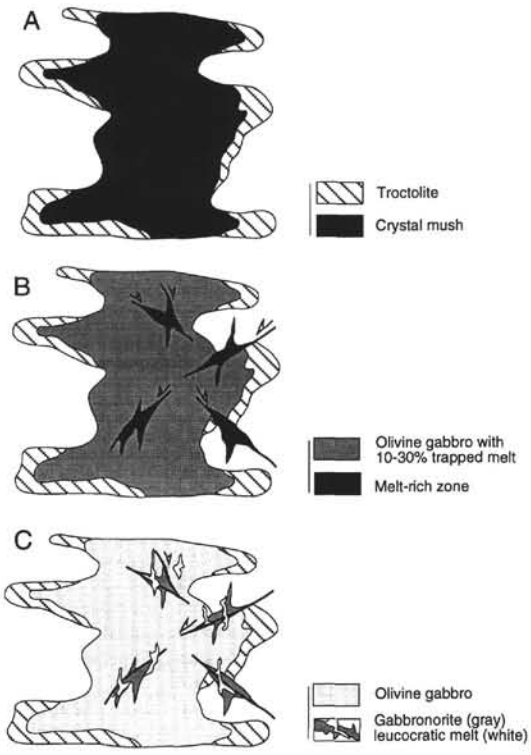

Figure 12. Schematic model, initially proposed by Bloomer et al. (1991) for the crystallization of gabbroic rocks at Site 735, and modified to fit the observations made on core from the MARK area. See text for an explanation of **A** through **C.**